

**Modeling of Convective-Stratiform Precipitation Processes:
Sensitivity to Partitioning Methods and Numerical Advection Schemes**

S. Lang^{1,2}, W.-K. Tao¹, J. Simpson¹ and B. Ferrier^{3,4}

¹*Laboratory for Atmospheres
NASA/Goddard Space Flight Center
Greenbelt, MD 20771*

²*Science Systems and Applications Inc.
Lanham, MD 20706*

³*NCEP/Environmental Modeling Centers
Washington, D. C. 20233*

⁴*General Sciences Corporation
Beltsville, MD 20705*

J. Applied Meteorology

(January 3, 2001)

Corresponding author address: Steve Lang, Mesoscale Atmospheric Processes
Branch, Code 912, NASA/GSFC, Greenbelt, MD 20771

Abstract

Six different convective-stratiform separation techniques, including a new technique that utilizes the ratio of vertical and terminal velocities, are compared and evaluated using two-dimensional numerical simulations of a tropical [Tropical Ocean Global Atmosphere Coupled Ocean-Atmosphere Response Experiment (TOGA COARE)] and midlatitude continental [Preliminary Regional Experiment for STORM-Central (PRESTORM)] squall line. The simulations are made using two different numerical advection schemes: 4th order and positive definite advection. Comparisons are made in terms of rainfall, cloud coverage, mass fluxes, apparent heating and moistening, mean hydrometeor profiles, CFADs (Contoured Frequency with Altitude Diagrams), microphysics, and latent heating retrieval. Overall, it was found that the different separation techniques produced results that qualitatively agreed. However, the quantitative differences were significant. Observational comparisons were unable to conclusively evaluate the performance of the techniques. Latent heating retrieval was shown to be sensitive to the use of separation technique mainly due to the stratiform region for methods that found very little stratiform rain. The midlatitude PRESTORM simulation was found to be nearly invariant with respect to advection type for most quantities while for TOGA COARE fourth order advection produced numerous shallow convective cores and positive definite advection fewer cells that were both broader and deeper penetrating above the freezing level.

1. Introduction

Squall lines are an important class of precipitating convective systems, often referred to as mesoscale convective systems or MCSs, that have long been the subject of study by the meteorological community. They occur both over land and water, and both in the tropics and midlatitudes. They can contribute a significant amount of rainfall to a particular region, produce severe weather, and impact the large scale environment. Squall lines consist of a linear group of thunderstorms or cumulonimbi usually along the leading edge of the system in the direction of propagation and, in the mature stage, an associated anvil containing a broad area of light precipitation. The precipitation in squall lines can generally be categorized as being either convective or stratiform in nature. There are several reasons for classifying the precipitation and its region of origin within the squall line. First, the mechanisms by which precipitation is formed are decidedly different in the two regions. The convective region is also generally associated with heavier precipitation rates. In addition, the latent heating profiles associated with each region are distinctly different from one another with each region having its own characteristic shape. The same is true for the mass flux and divergence profiles. Thus, it can be useful to distinguish the two regions for a variety of purposes. As such, a number of techniques have been developed over the years that are designed to separate convective systems, including squall lines, into their convective and stratiform components. The purpose of this study is to compare several of those techniques within the context of a numerical cloud resolving model in light of their potential applications.

An early study on tropical squall lines by Hamilton and Archbold (1945) described a typical squall line as a line of cumulonimbus clouds that preceded a broad downdraft region associated with a precipitating anvil that emanated from the cumulonimbus towers. In an early study on midlatitude squall lines, Newton (1950) constructed a time-height cross-section of a pre-frontal squall line showing a subsidence inversion behind the line using upper-air soundings from the Thunderstorm Project. Zipser (1977) looked into the kinematic structure of the squall line downdraft region using aircraft and sounding data gathered for a Caribbean squall line. He put forth a conceptual model wherein the downdraft region consisted of narrow near-saturated convective-scale downdrafts and a

broader unsaturated mesoscale downdraft that originated from mid-level inflow and was driven by rain evaporation. These two sources of downdrafts led to the formation of a stable layer behind the leading edge convection. Brown (1979) used a two-dimensional (2D) hydrostatic model with parameterized cumulus convection and simple microphysics to confirm this theory of an evaporatively driven mesoscale downdraft in the anvil region.

Houze (1977) had similar findings about the downdrafts in his study of a GATE squall line system to that of Zipser (1977). Using GATE radar data he computed the anvil percentage of the rainfall to be about 40%. He simply drew a boundary around the squall line region (i.e., the convective portion) and treated the rest as anvil. He noted the squall line had discrete cumulonimbus elements that formed the leading edge. New elements formed ahead of the system and merged with it. Later as they became older they blended into the stratiform anvil region. The precipitation falling from the anvil region was stratiform in nature as evidenced by a distinct radar bright band. First explained by Ryde (1946), the bright band is associated with broad areas of frozen light precipitation falling through the 0 C isotherm (Battan 1973; Atlas 1990).

Leary and Houze (1979) used radar data from several GATE cases to estimate cooling rates in and below the anvil bright band due to melting and rain evaporation. They found the horizontally uniform precipitation of the anvil region to contain rainfall rates on the order of 1 to 10 mm/h compared to 10 to 100 mm/h in the convective cores. Gamache and Houze (1982) obtained quantitative divergence and mass flux profiles for both the convective and anvil regions by compositing radar and wind data for a GATE squall line. The convective region contained low level convergence and upper level divergence while the anvil portion had mid-level convergence and divergence at both upper and lower levels. Net mass flux profiles were positive at all levels for the squall region while the anvil region showed positive fluxes aloft but downward fluxes below the base of the anvil. They separated the convective and anvil portions based on subjective assessment of the echo intensities, reflectivity gradients, the presence of vertical cores, and steadiness of the patterns. They found the squall-line echo to have an average width of 20 km. Churchill and Houze (1984), using aircraft data collected from a tropical cloud cluster during Winter MONEX, found much higher ice concentrations in the convective

region. The convective region was also dominated by rimed particles or graupel as opposed to aggregates in the anvil region.

An important aspect of squall line research involves their influence on the larger scale notably in the form of heating and moistening. Using a compositing technique, Reed and Recker (1971) estimated the average structure of 18 disturbances that crossed through a sounding network in the Marshall Islands. They obtained an estimate of the diabatic heating effects above 900 mb for a composite easterly wave disturbance. The difference between the trough and ridge positions showed positive heating effects throughout the troposphere with a maximum near 400 mb. Yanai *et al.* (1973) used a similar approach to estimate the apparent heating and moistening for tropical disturbances also observed in the Marshall Islands area. Their time averaged heating profile matched that of Recker and Reed (1971) fairly well with a single maximum in heating near 475 mb. These early estimates represented heating for an entire convective system. Houze (1982) used an idealized cloud system to put forth the first comprehensive estimates of the heating profiles associated with the convective and anvil regions by summing estimates of the cloud-scale terms. The convective profiles showed warming dominated by condensation throughout the depth of the troposphere. The anvil profiles had condensational warming in the middle and upper troposphere and cooling due to evaporation and melting in the lower troposphere. Johnson and Young (1983) computed the heating and moistening rates for tropical anvils using Winter MONEX data by computing the large-scale terms using soundings from a ship array when the array was covered mainly by mesoscale anvil clouds. Their results compared well with those of Houze (1982). Their anvil moistening profile showed moistening in the lower troposphere and drying aloft. Johnson (1984) partitioned the apparent heat and moisture source profiles of Yanai *et al.* (1973) into cumulus and mesoscale components by estimating the fraction of rainfall associated with the mesoscale anvil and using the anvil profiles of Johnson and Young (1983). The cumulus profiles were obtained as the residual. The resulting heating profile for the cumulus region matched fairly well with that of Houze (1982).

Tao and Soong (1986) used a three-dimensional (3D) numerical cloud model with warm rain microphysics to simulate a GATE rainband. They

produced heating and moistening profiles for the entire convective system similar to those from observational studies. Tao and Simpson (1989) added ice microphysics and a convective-stratiform separation technique based on Churchill and Houze (1984) to produce the first model simulated profiles of heating that distinguished the convective and anvil regions. These convective and anvil heating profiles were similar to those obtained by Houze (1982) and Johnson (1984). The simulations were based on a GATE composite case.

Recent studies (Simpson *et al.* 1988; Adler and Negri 1988; Tao *et al.* 1993a) have indicated that separation of convective and stratiform clouds is necessary for the successful retrieval of surface rain and latent heating profiles via remote sensing. Frank and McBride (1989) concluded that differences in the total heating profiles between AMEX and GATE cloud clusters were due to differences in the fraction of anvil rainfall. Using similar logic, Tao *et al.* (1993a) put forth an algorithm to retrieve the total mean latent heating profile for a system or region based on the rainfall, the percentage of rainfall that was stratiform and appropriate profiles of heating associated with the convective and stratiform regions. A higher stratiform percentage resulted in a more elevated level of maximum heating. The convective and stratiform heating profiles used in the algorithm could be obtained from both diagnostic and modeling studies of convective systems from various geographic regions. They indicated that the stratiform percentage should be to within 10% for an accurate retrieval. Alexander and Cotton (1998) recently devised a new mesoscale parameterization scheme to accompany a modified traditional cumulus parameterization scheme. They used the Tao *et al.* (1993b) convective- stratiform separation technique to select mesoscale profiles for their parameterization from cloud resolving model simulations of MCSs.

Recent cloud resolving modeling studies (e.g., Tao *et al.* 1993b; Xu 1995; Caniaux *et al.* 1994) have quantified the amount of stratiform rain as well as the heating and moisture budgets associated with the convective and stratiform regions of mesoscale convective systems using different techniques to separate the convective and stratiform regions. Current convective-stratiform separation for TRMM ground validation radars follows the algorithm of Steiner *et al.* (1995). Indeed the exact demarcation between convective and stratiform is somewhat arbitrary, but such separation has many useful applications. As such, it is

important to compare and contrast the various separation techniques that are available to numerical cloud models to determine whether similar conclusions are achieved and the magnitudes of any quantitative differences. This paper will help to address the issue by comparing five different convective-stratiform separation techniques that are currently being used plus an additional new method based on the premise that the terminal velocity of precipitation particles is large relative to the vertical velocity in regions of stratiform precipitation (e.g., Houghton 1968; Steiner *et al.* 1995; Houze 1997). These techniques are applied to two different cases: a well organized mid-latitude case (PRESTORM) and a well organized tropical case (TOGA COARE). Section 2 describes the model, the two cases, the separation techniques and two different types of numerical advection that will be used to further test the sensitivity of the model with regard to convective and stratiform differentiation. Section 3 compares the results of the numerical experiments in terms of rainfall, cloud coverage, mass fluxes, apparent heating and moistening, mean hydrometeor profiles, CFAD (Yuter and Houze 1995b) analyses, microphysics, and latent heating retrieval. Finally the summary and conclusions are given in Section 4.

2. Numerical Experiments

The model used in this study is the two-dimensional (2D) version of the Goddard Cumulus Ensemble (GCE) model. The GCE modeled flow is assumed anelastically balanced, filtering out sound waves by neglecting the local variation of air density with time in the mass equation. The cloud microphysics include a parameterized Kessler-type two-category liquid water scheme (cloud water and rain), and parameterized Lin *et al.* (1983) or Rutledge and Hobbs (1984) three-category ice-phase scheme (cloud ice, snow and hail/graupel). Short-wave (solar) and long-wave (infrared) radiation parameterizations as well as a subgrid-scale turbulence (one-and-a-half order) scheme are also included in the model. Details of the model description can be found in Tao and Simpson (1993) and Simpson and Tao (1993).

Two different cases, a well organized tropical oceanic squall system observed during TOGA COARE (Tropical Ocean Global Atmosphere Coupled Ocean-Atmosphere Response Experiment) and a well organized midlatitude continental squall system observed during PRESTORM (Preliminary Regional

Experiment for STORM-Central), will be used to test the various convective-stratiform partitioning methods and advection schemes described in Sections 2.1 and 2.2. The June 10-11, 1985 PRESTORM case has been well studied (e.g., Johnson and Hamilton 1988; Rutledge *et al.* 1988; Tao *et al.* 1993b; Tao *et al.* 1996). The PRESTORM environment contained a fair amount of instability but is also relatively dry when compared to the tropical environment. The thermodynamic profile used to initialize the model was a single sounding taken at 2330 UTC from Pratt, KS which was ahead of the newly forming squall line. The sounding is quite unstable with a lifted index of -5.37 and a CAPE of 2300 J/kg. The PRESTORM simulations were made using a modified shear profile [see Tao *et al.* (1993b)] and Lin *et al.* (1983) microphysics which are more representative of a hail environment usually associated with such strong continental systems. Observed reflectivities for this case were characteristically over 50 dBZ (Rutledge *et al.* 1988). A stretched vertical coordinate was used in the model with 31 grid points. The grid resolution ranged from 240 m at the lowest level to 1250 m at the top. The horizontal grid consisted of 1024 total grid points; the central 872 of which had a fixed 1 km resolution. The outer grids were stretched. Both long- and short-wave radiative parameterizations were used [see Tao *et al.* (1996)] though the majority of the simulation occurred during nighttime hours. There were no surface fluxes used in the model, and the time step was 6 seconds. The convective system was initiated using a low level cold pool. A cooling rate of 0.01 K/s was applied over a period of 10 minutes.

The February 22, 1993 TOGA COARE squall line has also been the subject of numerous studies. This system was observed with Doppler equipped instrumented aircraft (Jorgensen *et al.* 1997), and has been numerically simulated (Trier *et al.* 1996; Trier *et al.* 1997; Redelsperger *et al.* 2000; Wang *et al.* 1996, 2000). The sounding used to initialize the model for this case comes from LeMone *et al.* (1994). It is a composite sounding that consists of aircraft data below 6 km and a combination of the 1800 and 2400 UTC Honiara soundings above 6 km. The surface conditions are assumed to be: $P_{sfc}=1006$ mb, $T_{sfc}=28.66$ C, and $Q_{sfc}=23.2$ g/kg (Redelsperger *et al.* 2000). The resulting CAPE and lifted index values are moderately unstable at 1776 J/kg and -3.2, respectively. A low level westerly jet of 12 m/s is present near 2 km. The observed squall line propagated eastward and was oriented perpendicular to this jet feature. The squall line was initially linear but later evolved into a bow shape with a mid-level vortex along the

northern edge. Since this was an oceanic case, surface fluxes were included using the TOGA COARE flux algorithm put forth by Fairall *et al.* (1996). Additional information on the implementation of this algorithm into the GCE model can be found in Wang *et al.* (1996). The use of the TOGA COARE flux algorithm necessitates the use of a very fine first grid level. As such, a similar type of vertical stretching to that in the PRESTORM setup was used, but with the first grid level at 40 m. This in turn required a small time step of 5 seconds. Resolution at the highest model level was 1150 m. The horizontal grid followed that for the PRESTORM case but with a non-stretched resolution of 750 m and slightly smaller stretching. A modified version of the Rutledge and Hobbs (1984) 3-class ice scheme was used which is characteristic of graupel physics rather than hail. The shear above the low level jet at 2 km was reduced to allow for the development of a better stratiform region. Both solar and long-wave radiative fluxes were included as well. A low level cold pool similar to the PRESTORM case was used to start the convection. In addition, low level mesoscale lifting was applied in the TOGA COARE case. This lifting had a peak value of 3.4 cm/s near 1 km and was applied over the first 2 hours of the simulation. Table 1 shows some of the characteristics of the large scale environments associated with these two cases.

2.1 Numerical advection schemes

A second- or fourth-order horizontal advection scheme has generally been used in the model. However, using second-order or higher-order accuracy advection schemes can introduce some difficulties because negative values arise in the solution (Soong and Ogura 1973). This effect can be especially important in cases where the solution of the advection is used as input to nonlinear equations describing microphysical phenomena or inert tracers which can eventually lead to instability of the whole system (Smolarkiewicz 1983). The use of upstream differencing or other low-order schemes (Soong and Ogura 1973) would not produce dispersive "ripples" but would suffer from excessive numerical diffusion. Smolarkiewicz (1983) has reduced the implicit diffusion by using a second "upstream" step where a specifically defined velocity field leads to a new form of a positive definite advection scheme with small implicit diffusion. The positive definite advection scheme involves iterations and needs more computational resources. This scheme has been improved to include

multidimensional applications (Smolarkiewicz 1984) and a non-oscillatory option (Smolarkiewicz and Grabowski 1990).

The GCE model has implemented this Multi-dimensional Positive Definite Advection Transport Algorithm (MPDATA). Two specific solutions are performed in this study. The first one has all scalar variables (potential temperature, water vapor, turbulent coefficient and all five hydrometeor classes) use forward time differencing and the MPDATA for advection. The dynamic variables, u , v and w , use a second-order accurate advection scheme and a leapfrog time integration (kinetic energy semi-conserving method). The second more traditional approach uses leapfrog time integration and a fourth-order space derivative scheme for scalar and dynamic variables.

2.2 Convection-Stratiform Partitioning Methods

(a) Churchill and Houze (1984)

Churchill and Houze (1984) designed a method to partition convective and stratiform regions using radar estimated rainfall rates. Their technique was based on an assumption from a previous work by Houze (1973) that convective cells have peak rainfall rates that are at least twice as large as the surrounding background. Consequently, they identified convective cores as points whose rainfall rates were at least twice that of the surrounding 400 km². For each core, the surrounding 150 km² was also deemed convective. Finally, any rainfall rate greater than 20 mm/h (~40 dBZ) was also made convective. Originally, Churchill and Houze (1984) applied their method to radar data at a 3 km altitude with a 4 km horizontal resolution. In the GCE model, this technique is applied to surface rainfall rates and normally on a higher resolution grid reducing the size of the background area (2 points in each direction). Also, the 20 mm/h convective threshold is allowed to vary between 10 and 25 mm/h depending on the time of the simulation. This method is termed the "C&H method" hereafter.

(b) Tao and Simpson (1989) and Tao *et al.* (1993b)

In this convective-stratiform partitioning method, convective, stratiform and non-surface precipitating regions are identified using the information from

surface rainrate first (C&H method). Two additional criteria are applied which have been included to identify regions where convection may be quite active aloft though there is little or no precipitation yet at the surface, such as areas associated with tilted updrafts and new cells initiated ahead of organized squall lines (Tao et al. 1993b). Non-surface precipitation regions are considered to be convective if cloud water exceeds a specific threshold (i.e., the maximum of either 0.5 g kg^{-1} or half of the maximum cloud water content at that specific simulation time), or if the updraft exceeds a specific threshold (i.e., 3 m s^{-1}) below the melting level. The presence of this amount of cloud water is a good indication of a saturated area (100% Relative humidity). For the region classified as stratiform by the C&H method, additional criteria are considered to identify active convective cells aloft. First the updraft velocity is checked above the melting level. If it exceeds the maximum between 5 m/s and half of the maximum updraft value at that simulation time, the column is considered convective. Second cloud water and cloud ice content above the melting level are also checked. If their combined value exceeds the maximum between 1.5 g/kg or half of their maximum combined content at that simulation time, the column is also convective.

These thresholds are obtained by examining the modeled cloud structures thoroughly. However, these threshold values may need to be adjusted for different cloud systems as well as for the various stages of their life cycle.

Cloudy regions ahead of the gust front are also classified as convective in order to achieve coherent areas of convective and stratiform rainfall. This method is termed the "GCE method" and has been adapted by Chin (1994) and Alexander and Cotton (1998).

(c) Xu (1995)

A third convective-stratiform partitioning method was applied to a cloud ensemble simulation by Xu (1995). This method's idea is very similar to the one developed by Churchill and Houze (1984), except that the horizontal gradient of absolute air vertical velocity below the melting level rather than rainfall is used. Model grid points that have a vertical velocity twice as large as the averaged value taken over the four surrounding grid points are identified as convective

cell cores. For each core grid point, the grid point residing on either side is also made convective. Furthermore, any grid point with a rainrate in excess of 25 mm/h or an absolute vertical velocity in excess of 3 m/s is designated as convective regardless of the above criteria. The remaining columns where the total liquid water path exceeds 0.2 kg/m² are then defined as stratiform. The stratiform columns are then further checked for shallow convection. Columns that have cloud water paths above 0.4 kg/m², rain water paths below 0.1 kg/m² and mean upward motion all below the melting layer are made convective. However, in this study, any areas with surface precipitation that were not found to be convective by the first three criteria (i.e., vertical velocity gradients, vertical velocity thresholds, and surface precipitation thresholds) were considered to be the stratiform region. In addition, the surface rainrate threshold was not fixed at 25 mm/h but was allowed to vary between 10 and 25 mm/h depending on the simulation time. One other modification involves the 3 m/s vertical velocity threshold. In the GCE model it is taken to be the minimum between 3 m/s and one fourth of the maximum vertical velocity at that simulation time. Again, these modifications consider the resolution of cloud characteristics during its life time. This method is termed the "Xu method".

(d) Caniaux *et al.* (1994)

In this method, a characteristic width or fixed number of model grid points (e.g., 20-40) are centered on the maximum surface rainrate and designated as the convective region. Remaining grid points with surface precipitation comprise the stratiform region. This method is termed the "constant area or CA method". In this study, the convective region was fixed at a width of 20 km, so it is referred to as the "CA20 method".

(e) Steiner *et al.* (1995)

This method is a texture algorithm applied to radar reflectivities at a level below the melting band and is an extension of the earlier C&H method. Reflectivities are compared against a background average taken over a radius of 11 km. Points that exceed the background average by a certain threshold are made convective. The threshold varies as a function of the background average. In addition, any gridpoint that exceeds 40 dBZ is made convective. Finally, for

each of the gridpoints identified as convective, a surrounding area which depends upon the intensity of the core gridpoint is made convective. The remaining rainy areas are then stratiform.

(f) Vt-W Method

In this study, a new method is introduced. This method is based on the basic premise that the terminal velocity of precipitation particles is large relative to the vertical velocity in regions of stratiform precipitation (e.g., Houghton 1968; Steiner *et al.* 1995; Houze 1997). As such, the magnitude of the terminal velocity is compared to the magnitude of the vertical velocity. If the ratio of the terminal velocity's magnitude to the vertical velocity's magnitude exceeds the square root of an order of magnitude (i.e., 3.16), the grid point is considered to satisfy stratiform conditions. Only regions of the cloud volume where the magnitudes of the terminal velocity and vertical velocity exceed 2 and 1 m/s, respectively, are examined in order to avoid areas along the cloud boundaries where the magnitudes involved are quite small but the ratios large. Above the melting layer, only positive values of W are used in the ratio. Finally, below the melting layer, in order to capture new convective updrafts that may not yet have substantial hydrometeor fallspeeds, any point that has a vertical velocity of at least 1 m/s and 0.1 g/kg of cloud water present is considered convective.

In this study, two criteria that have been adopted in the GCE method are applied at the end of all of the other convective-stratiform partitioning methods as well. First, surface rainfall rates are thresholded. The threshold is allowed to vary between 10 and 25 mm/h depending on the simulation time. Within the first hour, the threshold is allowed to vary between 10 and 15 mm/h, and after three hours it is allowed to vary between 20 and 25 mm/h depending on what the maximum surface rainrate is at that particular time. Any grid column with a surface rainfall rate that exceeds the threshold is automatically made convective if it already is not. And secondly, an attempt is made to make the convective and stratiform regions coherent. This is accomplished by first making all cloudy areas ahead of the gust front convective. Next, any cloudy areas that are in front of the last stratiform point (in the direction of storm motion) but behind the back edge of the convective region are made stratiform. Then, any points classified as stratiform that are in front of the leading edge of the convective region are made

convective. And finally, if the convective region is 5 grid points or less in width, any stratiform points that fall in between are made convective.

Table 2 lists the characteristics of the various convective-stratiform partitioning methods.

3. Results and Discussion

Model simulations were made for 720 minutes for both the PRESTORM and TOGA COARE cases using both Positive Definite Advection (PDA) and fourth-order advection (4th) in each case for a total of four experiments. Figure 1 shows the vertical cross-sections of estimated radar reflectivity at minute 720 for all the runs. All the simulations show a classical squall-line structure (e.g., Gamache and Houze 1982) with a leading convective edge, trailing stratiform region with a bright band, and new cell growth just ahead of the leading edge as the system propagates forward. Reflectivities exceed 50 dBZ and regularly reach 60 dBZ in the convective cores of the PRESTORM case for both types of advection. In terms of the stratiform region, the 4th order run actually produces on average a slightly broader area of stratiform rain. However, the most notable difference between the 4th order and PDA can be seen in the variability of the reflectivity field in the stratiform region. Not only does the PDA run appear smoother, but the reflectivity features are also more coherent. The 4th order run shows a lot of small scale variation not present in the PDA run¹.

Looking at the TOGA COARE case, many of these same characteristics are evident, though there are some differences. Core reflectivities do frequently exceed 50 dBZ but never 60 dBZ, and the 50 dBZ values are for the most part restricted to below 3 km, unlike in the midlatitude case where they can reach upwards of 6 km. Again, the 4th order run produces a broader area of stratiform rainfall, but there are also significant differences in the convective region. The 4th order run tends to produce numerous shallow convective cores that are

¹ As will be seen later in the TOGA COARE hydrometeor profiles, 4th order advection can lead to vertical oscillations in the hydrometeor fields, namely graupel and snow, not present with PDA. This was also found in another current GCE modeling study by Johnson *et al.* (2001).

narrow and spaced close together, while the PDA run generates fewer cells that are both broader and more likely to penetrate further above the freezing level. The sensitivity to advection in the TOGA COARE case not seen in PRESTORM may be due to the weaker instability in the tropics that would allow subtle differences in advection to have more of an effect. The PDA results agree more favorably with the observed Doppler derived reflectivity and vertical velocity structures (Jorgensen *et al.* 1997). Compared to the PRESTORM case, the transition from convective to stratiform rain does not appear to be as definitive. This is due to the succession of numerous small cells in the tropical case that do not significantly penetrate the freezing level, especially with 4th order advection. In contrast, the leading convective cells in the PRESTORM case penetrate well above the freezing where hydrometeors are then more likely to be carried rearward to form a more discernable bright band.

Time-domain cross-sections of surface rainfall, or Hov-Muller diagrams, are presented in Figure 2 for all four simulations. All runs show a change in forward propagation speed as the systems mature. The system almost discretely jumps to a faster propagation speed at 180 minutes for the PRESTORM case with 4th order advection. The evolution to a faster propagation speed is similar for the PRESTORM PDA run, but the transition is smoother. The shift in propagation speed is also accompanied by a broadening of the stratiform region (more evident in the 4th order run). The systems are likely transitioning from an erect updraft profile to an upshear profile (Ferrier *et al.* 1996). As for the TOGA COARE runs, there is a slight forward acceleration evident after about 150 minutes in the 4th order run while the PDA run shows a much sharper increase at 270 minutes. Also, the system propagates approximately 0.58 m/s faster using PDA. The forward propagation speeds were nearly identical for both 4th order and PDA for the PRESTORM case.

3.1 Rainfall Statistics

Table 3 shows the total amount of rainfall per grid point accumulated over all 12 hours of simulation time for all four runs. The totals are similar for each case. In the PRESTORM case, PDA produces 1.9% less rainfall than 4th order advection, while PDA produces just 1.4% less rainfall in the TOGA COARE case. Figure 3a shows time series of instantaneous grid averaged total and stratiform

rainfall for both PDA and 4th order runs for the PRESTORM case. The stratiform amount is obtained via the GCE separation method. The stratiform amounts match closely and slowly increase throughout the simulation. Total amounts are also quite similar, except for a few distinct episodes of increased rainfall near 200 and just before 360 minutes in the 4th order run and just after 480 minutes in the PDA simulation. Looking at the Hov-Muller diagrams in Fig. 2, these episodes can usually be traced to periods when cells develop ahead of the main line and then merge with the system. This merging can lead to enhanced rainfall (Byers and Braham 1949; Simpson 1980; Wescott 1984; Tao and Simpson 1984, 1989).

Figure 3b shows the same instantaneous grid point averaged total and stratiform rainfall traces but for the TOGA COARE case. The 4th order run has a period of higher rainfall from 120 to 240 minutes followed by a period of higher rainfall in the PDA run. The PDA run also has more rainfall in the stratiform region from about minute 300 to minute 420 which can be attributed to a few cells that persist with greater intensity behind the leading edge in the PDA run. Stratiform rain increases more rapidly than in the PRESTORM case then levels off.

Results from the various convective-stratiform separation techniques are also shown in Table 3. For the PRESTORM case, the C&H method has the most stratiform rain with the GCE and CA20 methods close behind. The Xu method then detects a modest amount, while the Vt-W and Steiner methods find very small amounts of stratiform rain. The results do not vary significantly relative to the type of advective scheme used. The GCE, C&H, and CA20 methods all give pretty similar results for both types of advection. These range from 16.9 to 21.5% stratiform rain inclusive of both advection types. Johnson and Hamilton (1988) reported an average stratiform rain amount of 29% for this PRESTORM case using surface rain gauge data. As the system matures, the stratiform percentage increases both for the model results and the observations. If the stratiform rain percentage is computed over the final 240 minutes of the simulation, during the mature stage, for the PDA run, the GCE, C&H, Xu, and CA20 estimated percentages increase around 10% while Steiner and Vt-W increase only 2-5%. Johnson and Hamilton (1988) estimated the observed mature stage stratiform component to be between 30 and 40%. This makes all of

the methods appear too low in their estimates of stratiform percentage though the GCE, C&H and CA20 values are reasonably close especially for the mature stage. However, Johnson and Hamilton (1988) simply assigned rainrates in excess of 6 mm/h as convective in their analysis of the mesonet rain gauge data. Applying this same criteria to the model simulations results in a stratiform rain percentage of just 4.2% for the PDA run, which is now in very close agreement with the Steiner and Vt-W estimates. Obviously the rainfall distribution in the model does not match the observations. Sui et al. (1998) found similar problems with the model versus observed rainfall. This makes evaluating the relative performance of the separation methods using the model versus observed stratiform percentages problematic.

In the TOGA COARE case, all of the methods are consistent in finding higher stratiform amounts in the PDA run (3-8% more). This time it is the GCE, C&H, and Xu methods that yield similar amounts of stratiform rain, about 35 to 42% for the 4th order run and about 42 to 49% for PDA. The CA20 method shows around 30% and now ranks lower (less than Xu) in a relative sense compared with the PRESTORM case. The Vt-W and Steiner methods still give the least amount of stratiform rain, less than 20% for the TOGA COARE simulations. Short et al. (1997) reported that 40% of the rainfall that occurred during active periods in TOGA COARE was stratiform. Active periods are associated more with organized types of convection. They used a texture algorithm similar to the Steiner method to separate rain maps derived from shipboard radar data into convective and stratiform portions. This makes the GCE, C&H, and Xu methods appear favorably close to observations in the TOGA COARE case. Of course, the same issue of how well the model replicates the observed rainfall distribution remains.

For both the PRESTORM and TOGA COARE cases, the Steiner method consistently produces the least amount of stratiform rain and could appear to significantly underestimate the amount of stratiform rain. One factor pertains to the grid resolutions in the model simulations. The Steiner method was designed for a grid resolution of 2 km, whereas the model has a 1 km resolution in the PRESTORM case and a 0.75 km resolution for TOGA COARE. If the method is applied to a grid with a higher resolution than what it was originally designed for, it will detect small scale deviations and identify them as convective

thus overestimating the amount of convective rain (Steiner et al. 1995). Steiner et al. (1995) recommend applying the technique at a level below the bright band but not too low so as to allow for greater radar coverage. They also recommend using a lower level in mid-latitudes to account for possible evaporative effects. In the model, there is no radar restriction, but nonetheless a level of 1.8 km was used in both the PRESTORM and TOGA COARE cases. This relatively low level means that evaporation is likely to be small. Nevertheless in its current application, in the PRESTORM case, regions that the method identifies as convective are always close to areas of at least 40 dBZ (Fig. 1). And, in the TOGA COARE case, the difference between the Steiner method and most of the others is in the treatment of the cells that are behind the leading edge. These are more likely to be identified as convective by the Steiner method and Vt-W methods. Occasionally the GCE and Xu methods identify parts of these as convective too (Fig. 1). So, based on the simulated reflectivity structures and the possible bias towards high rainrates in the model, the Steiner method appears to perform reasonably.

3.2 *Area Cloud Coverage*

Vertical profiles of cloud coverage are shown in Fig. 4 for both types of advection for each case. Grid points that had total hydrometeor contents in excess of 0.01 g/m³ were considered cloudy. In the PRESTORM case, below 7 km the profiles are very similar, while at upper levels, on average, the PDA run shows a broader area that is associated with the non-surface-precipitating portion of the anvil. The difference is largest at 12 km, on the top portion of the anvil. The mean width of the cloudy area is 280 km for 4th order advection while PDA averages 304 km. In the TOGA COARE case, the situation is similar with the two profiles nearly identical below about 5.5 km and PDA broader above that level. The average cloud areas in the TOGA COARE case are 142 km for 4th order and 161 km for PDA. In addition, average cloudtops in the PDA run are a kilometer higher. This is likely a result of the taller more vigorous nature of the cells in the PDA simulation that allows more condensate to penetrate higher above the freezing level.

Time series of convective and stratiform rain area (not shown) were computed for both cases and both advection types using each of the separation

techniques. In the PRESTORM case, there is an overall trend for the stratiform area to slowly but steadily increase in size. The increase flattens out over the final 2 hours of simulation time. The average mean width of the stratiform region over the 12 hour simulation time for all 6 methods was 47 km for 4th order and 43 km for PDA (Table 4). In the PDA run the mean 12 hour stratiform width ranged from 50 km for the C&H method to 29 km for Vt-W. Convective area increased much more rapidly. The growth tapered off a little more quickly in the 4th order run. The resulting mean width of the convective region for the 12 hour simulation time was 81 km for 4th order and 95 km for PDA. The average convective width varied from 87 km for C&H to 110 km for Vt-W in the PDA run. Because the coherence approach was applied, the CA20 method produced an average convective width of 91 km for the PDA run due to the forward anvil. This agrees quite well with the ensemble average.

The TOGA COARE runs reveal a similar trend in the stratiform area to the PRESTORM runs, a slow steady increase over the course of the simulation. The resulting average mean 12 hour stratiform width for the 4th order and PDA runs (Table 4) was 62 and 56 km, respectively. In the PDA run, the mean 12 hour width varied from 43 km for Vt-W up to 67 km for C&H. The convective width in the TOGA COARE runs increased more slowly than in the PRESTORM case and leveled off much sooner at a much smaller characteristic width (partially due to the forward anvil in the PRESTORM case). The 12 hour mean average values were 20 km for 4th order and 27 km for PDA for TOGA COARE. So in both cases the convective ratio was slightly higher for PDA. The characteristic 20 km convective width assumed in the CA20 approach yields 12 hour means that in the tropical case again agree quite well with the ensemble, 21 and 28 km respectively for 4th order and PDA.

3.3 *Cloud Mass Fluxes*

Accumulated mass fluxes for the PRESTORM case are shown in Fig. 5a for both types of advection. The fluxes are subdivided into convective and anvil regions using the GCE method. The convective profiles are fairly similar showing positive at all levels with a single maximum in the 4 to 5 km range. Though the maximum is larger for the PDA run, at upper levels, the 4th order convective profile is larger. In the anvil region, both schemes show single peaks

in upward fluxes at 9 km and single downward peaks between 2 and 3 km. Aloft, the upward peak is larger for PDA while at low levels the two schemes produce similar downward peaks but at slightly different levels. If the convective and anvil fluxes are combined however, the total profiles are nearly identical at all levels for both types of advection suggesting the differences in the component profiles may be attributed to the convective-stratiform partitioning. Time-height cross-sections of maximum downdrafts (not shown) reveal that peak updrafts are found initially around 9 km during the early stages of the simulations then transition down to 4 km over the later stages for both types of advection.

The mass flux profiles for the two TOGA COARE simulations are shown in Fig. 5b. The convective and anvil profiles, again using the GCE separation method, are generally similar to those found in PRESTORM. The convective peaks are sharper and lower around 2 to 3 km, about the same level as the downward peaks in the anvil profiles. If the components are combined however, the total accumulated profiles do show some differences. Between 2 and 6 km, there are more net upward fluxes in the 4th order run. At upper levels in the anvil region, the PDA simulation contains significantly more upward fluxes. These additional fluxes are associated with cells behind the leading edge that are much more vigorous in the PDA run. Time-height cross-sections of maximum updrafts (not shown) indicate that after 240 minutes, peak updrafts occasionally exceed 3 m/s in the 4th order run above the freezing level but are usually on the order of 1 to 2 m/s. On the contrary, the PDA simulation contains updrafts regularly on the order of 3 m/s but sometimes as high as 5 to 7 m/s above the freezing level. Furthermore, in the PDA run, a few 2 to 3 m/s updrafts are able to penetrate above 13 and 14 km, whereas after 240 minutes, 2 m/s updrafts in the 4th order run are confined below 13 km.

Figure 6a shows profiles of accumulated mass flux separated into convective and anvil components for the PDA PRESTORM run using each of the six different separation techniques. All of the profiles are qualitatively similar, and the results appear independent of the advection type. The convective profiles all show net upward mass flux throughout the depth of the troposphere with a single maximum. The anvil profiles all show net upward mass flux in the upper troposphere and net downward mass flux in the lower troposphere. The heights and magnitudes of the maxima vary significantly from

technique to technique. The height of the convective maximum varies between 3.5 and 6 km while the magnitude varies between 110 and 130 g/cm²/grid. The stratiform maxima have comparable differences in height but even greater variation in magnitude. In general, the techniques behave as expected especially at middle and upper levels where the Vt-W method has the convective profile with the most upward mass flux and the C&H convective profile has the least. The other methods fall in between in the same relative sequence as their stratiform areas except for the CA20 method which differs significantly from the rest especially at low levels. Based on cross-sections of vertical velocity, there is evidence for two main downdrafts behind the leading edge updraft. The first downdraft is located about 5-10 km to the rear of the leading edge updraft, and the second is generally about 20-25 km behind. All the methods include the first downdraft nearest the leading edge updraft as part of the convective region. The convective area of the CA20 method does not reach to the second downdraft while the other methods occasionally include it as part of their convective regime. This accounts for the larger negative mass fluxes in the low level anvil profiles of the CA20 method compared to the others. With the second main area of downdrafts effectively in the anvil region, the low level convective region of the CA20 method shows more net upward fluxes resulting in a maximum at lower levels. Some of the methods include some very strong updrafts aloft as part of the upward mass flux in the their anvil region [see Section 3.6].

Compared to the PRESTORM profiles, the TOGA COARE convective and anvil mass flux profiles generated by the various separation techniques (Fig. 6b) are less variable at low levels but more variable aloft. Again, the results are consistent for both types of advection. Almost all of the methods place the convective peak upward mass flux at a level of 2.5 km. The peak convective magnitudes vary from 40 to 65 g/cm²/grid. Likewise the low-level downward fluxes in the anvil profiles are also quite similar. The GCE, C&H, and CA20 methods have nearly identical convective and anvil profiles throughout the depth of the system. The real variation between the methods appears aloft, above the freezing level. The Xu, Steiner, and Vt-W methods increasingly categorize upward mass fluxes above the melting level as convective whereas the other three have slightly negative net convective mass flux above the melting level. The Xu method is based on vertical velocities. Occasionally vertical velocities near the freezing level and to the rear of the leading edge were

sufficient to satisfy the convective requirements stipulated in the Xu method. These updrafts were associated with cells behind the leading edge. While the Xu method categorized parts of these cells as convective from time to time, the Steiner method was more likely to identify them as convective based on their reflectivity structure. Frequently these cells contained updrafts aloft that were on the order of 1 to 2 m/s. Consequently, the Vt-W method was most likely to categorize these cells as convective leading to a fairly large diversity among the profiles above the freezing level including changes in shape.

3.4 *Apparent Heating (Q_1) and Moistening (Q_2)*

Q_1 profiles between 4th order and PDA in the PRESTORM case are nearly identical. Figure 7a shows that the total heating matches over the complete depth of the troposphere for the two different advection types. The total heating shows a double maxima with a mid-level maximum at 7 km and a smaller secondary one near 13 km. There is heating throughout the depth of the troposphere but cooling above the tropopause near 15 km. The convective and anvil heating profiles, partitioned according to the GCE method, are also almost identical. The convective profiles show predominantly heating throughout with a main maximum near 5.5 km. A relatively weak secondary maximum is evident near 12 km, and the cooling above the tropopause is minimal. The anvil profiles show cooling below 5 km, though the freezing level is near 4 km, and heating aloft with the largest maximum near 9 km and a secondary one nearly as large near 14 km. The cooling above the tropopause is more pronounced than in the convective profiles. All of the profiles have been normalized with respect to total surface rainfall.

Convective and anvil profiles for PDA are broken down into their individual components in Fig. 8a&b. The convective components are quite similar for the two types of advection. Condensation is the dominant term with a maximum near 4 km, close to the freezing level. Above this level, condensation drops off while deposition, the second largest term, increases to a maximum near 9 km. Sublimation is relatively small and peaks at the same level as deposition. Evaporation increases towards the ground and becomes larger than condensation only near the surface. Freezing and melting are combined into one curve and are of equal magnitude on either side of the

freezing level. The weak secondary maximum in heating near 12 km is attributed to eddy flux convergence. This term is also responsible for the cooling above the tropopause. It is also a relatively important term near the freezing level and again near the surface. Radiation effects are negligible in the convective region.

The anvil components, shown in Fig. 8b, are also similar for both types of advection except around 9 km. Condensation is still significant, but deposition and sublimation are now the dominant terms. Condensation is fairly uniform from about 1 to 8 km. Evaporation is quite weak above 4 km but is the dominant term below 3.5 km. Deposition dominates the heating above 6 km, but it is nearly compensated for by sublimation. The peak values in deposition and sublimation are much greater in the PDA run. However, the net difference between the two is the same as the 4th order run resulting in the same net heating. Freezing is negligible while melting is significant over a 2 km depth below the melting level. The eddy flux term is significant below the melting level, but is quite large around the tropopause. It alone is responsible for the elevated secondary peak in anvil heating and also for the large cooling seen above the tropopause. The radiation term does show cloud top cooling and cloud base warming in association with the anvil, but it is still in comparison a relatively minor term in the anvil region.

Unlike the PRESTORM case, the TOGA COARE Q1 profiles for the two advection schemes do show some differences (Fig. 7b). Again using the GCE separation method, the convective profiles have similar shapes but the 4th order profile has a larger magnitude of peak heating around 3 km. The anvil profiles are similar below 10 km, but above that level the PDA profile shows significantly more heating. These differences are reflected in the total heating profiles. Compared to the PRESTORM profiles, the TOGA COARE convective profiles show a similar magnitude in peak heating when normalized with respect to surface rainfall, but the elevation of the peak is much lower near 3.0 km compared to 5.5 km in the PRESTORM case. Also, whereas the PRESTORM convective profiles were nearly all heating, the TOGA COARE profiles do show some significant cooling from 7 to 12 km above the lower level heating. But unlike the PRESTORM case, there is no strong heating or cooling associated with the tropopause. The anvil profiles show strong cooling, stronger than in the

PRESTORM case, from below 4 km down to almost the surface. The peak heating aloft is also stronger than in PRESTORM though at about the same level, 7-9 km. This heating instead shows up in the convective profiles for PRESTORM.

The convective components for the PDA TOGA COARE profiles, shown in Fig. 8c, are similar to the PRESTORM components in that condensation is the dominant term. However, in the tropical case this term is so dominant that most of the other terms are practically insignificant by comparison. With a higher freezing level and weaker instability in the tropics, deposition and hence sublimation become far less important. The same is true for freezing and melting. The moister environment also helps to reduce evaporation in the convective region though it is non-negligible. The eddy flux term is smaller too compared to the midlatitude system. As with the PRESTORM case, the convective components are independent of the advection.

Figure 8d shows the anvil Q1 components for the PDA TOGA COARE simulation. Heating is almost evenly divided between condensation below and deposition aloft while sublimation is far smaller than in the PRESTORM case. Eddy fluxes are slightly weaker than for PRESTORM, but evaporation is quite large below 5 km. Above 9 km, deposition and to a lesser degree sublimation are greater with PDA. Radiational cloud-base warming is also larger and shifted upward by 1 km in the PDA simulation. Likewise eddy flux warming just above cloud top is stronger and 1 km higher. This is consistent with the taller cells in the PDA simulation for TOGA COARE.

Normalized convective and stratiform Q1 profiles from the various separation techniques are shown in Fig. 9a&b for the PRESTORM case. Again, the results are similar for both types of advection. The overall shapes of the profiles are very similar between the methods with the only real differences being in the magnitudes at mid-levels. Mid-levels are where the greatest variation exists; Steiner and Vt-W have the largest convective heating (and smallest anvil heating) while C&H has the least. The Xu, GCE, and CA20 methods fall in between in descending order of convective heating. The biggest differences are at 7 km in the 4th order run where convective heating ranges from 0.75 (deg/mm) for the Steiner and Vt-W methods down to 0.43 for C&H.

Below the melting level and above 9 km, the methods are all very close with maximum differences on the order of 0.1 (deg/mm).

Results from the two TOGA COARE simulations are shown in Fig. 9c&d. The separation techniques show very close agreement below the melting level. The narrowness of the results in this region can be attributed to the lack of any strong microphysically induced heating or cooling beyond the vicinity of the leading convective edge. Since all of the methods assign the region in and around the leading edge as convective, there is very little variation in the results even though the convective areas may differ significantly. Unlike the PRESTORM case where strong pockets of cooling, due to evaporation or even melting, can exist well behind the leading edge below the melting level, the moist environment of the tropics mitigates this effect. Hence the Steiner and Vt-W methods, which on average have significantly larger convective regions, yield only slightly less cooling in the anvil region compared to the other methods below the melting level. The results are different at middle and upper levels. The GCE, CA20 and C&H methods all produce similar convective and anvil heating above the freezing level. The Xu method differs slightly from these assigning more of the heating aloft to the convective region. The Steiner method is next with even more of the heating as convective, while Vt-W has the most heating aloft in the convective profiles noticeably more than even Steiner. This is different from the PRESTORM case where the two methods are nearly identical at all levels. Unlike below the melting level, there are regions of significant heating aloft to the rear of the leading convective edge where there are pockets of condensational and depositional heating associated with old cells to the rear of the leading edge.

Comparing the Q2 profiles for the two PRESTORM runs (Fig. 10a) shows that total moistening for 4th order and PDA is nearly identical. The convective and anvil profiles are also very similar. The TOGA COARE Q2 profiles (Fig. 10b) are also quite similar between 4th order and PDA. The anvil profiles are a very close match while 4th order has slightly more drying between 2 and 4 km in the convective profile and hence the total profile. Both of the TOGA COARE anvil profiles show moistening below 4.5 km, similar to the PRESTORM profiles only stronger. Both the TOGA COARE and PRESTORM convective profiles show drying mainly below 4.5 km with similar peak magnitudes. The TOGA COARE

profiles peak near 3.5 km while the PRESTORM profiles peak closer to 2 km.

The convective and anvil Q2 profiles show greater variation in the PRESTORM case than in the TOGA COARE case (Fig. 11). This is again due to the lack of strong microphysics behind the leading edge below the melting level in the TOGA COARE case where Q2 has its largest amplitude. Most of the methods are in close agreement in the PRESTORM case except for CA20. The CA20 method shows the largest deviation from the other methods with the strongest anvil moistening and convective drying for both runs. All six separation techniques are similar to each other in the two TOGA COARE simulations below 4 km differ slightly at middle levels, however.

3.5 *Hydrometeor Profiles*

Total hydrometeor profiles for both forms of advection and both cases are shown in Fig. 12. The two PRESTORM runs show very close agreement for all five hydrometeor species. The snow profile for 4th order advection has a slightly larger peak value. The TOGA COARE runs show more variation. At low levels, the 4th order rain and cloud profiles are slightly larger though the shapes are similar. Mid-level graupel contents are higher in the 4th order run, but aloft the PDA snow, graupel and cloud ice contents are substantially larger which is consistent with the deeper cell structure. Also, the PDA graupel and snow profiles are much smoother.

The GCE method is the only one that directly utilizes hydrometeor data to help differentiate between convective and stratiform areas. Though difficult to obtain in real world applications, it can be useful for identifying convective regions. Large values of cloud water or cloud ice are associated with significant updrafts that are identified with convection. Total hydrometeor profiles for the convective and anvil regions were computed for each technique (not shown). Differences in cloud water content between the various methods for the PRESTORM case are not very large. The Steiner and Vt-W methods have the most convective cloud water (97%) while C&H has the least (74%). The GCE method is in the middle (84%). In all of the methods, the percentage of cloud water that is convective is high. Aloft, cloud ice is roughly equally divided between convective and anvil. Values range from 83% convective for Vt-W to

only 47% convective for C&H. Another indication of convection is the presence of hail. For the Vt-W and Steiner methods, around 85% of the hail falls within the convective region; for Xu it is 68%, for the GCE and CA20 methods, about 58%, and for C&H, only 50%. The behavior between PDA and 4th order advection is the same.

In the case of TOGA COARE, nearly all of the cloud water below 3 km (2 km for PDA) is found to be convective in all the methods. Cloud water is present at mid-levels in both the PRESTORM and the TOGA COARE case, but unlike the PRESTORM case, there is a lot of variation between the techniques regarding the mid-level cloud water. This is due to the the presence of significant amounts of cloud water further behind the leading edge in TOGA COARE. Cloud water ranges from just 48% convective in the C&H method up to 88% for Steiner. GCE has around 60%. The GCE, C&H, and CA20 methods have essentially no convective cloud ice (less than 7%) with Xu only a small amount, about 12%. The Steiner method has a fair amount with 37% while the Vt-W method has the most at 47%. The values are for the 4th order run; the PDA results are similar.

3.6 *Contoured Frequency with Altitude Diagrams (CFADs)*

CFADs are frequency distributions at each altitude summed together as a function of height to make a statistical diagram of a particular field (Yuter and Houze 1995b). Steiner et al. (1995) constructed CFADs of radar reflectivity from Darwin, Australia, for convective, anvil, and total storm volumes for the entire month of February 1998 to verify their convective-stratiform separation scheme (i.e., the Steiner method). A narrower distribution with peaks at lower magnitudes (especially at low levels) is expected for the stratiform region, which they found. They also tested their separation algorithm by computing CFADs on data from a CaPE (Convection and Precipitation/Electrification Experiment) case where doppler derived vertical velocities were available. They found that the velocities were consistent in showing a much narrower CFAD for the stratiform region and a broad convective CFAD having a significant portion of the vertical velocities greater than ± 5 m/s. The corresponding reflectivity CFADs were also compatible with those generated for the Darwin data.

CFADs were constructed for both the PRESTORM and TOGA COARE cases for each of the various separation algorithms. The PRESTORM results indicate that each of the algorithms was able to produce convective and stratiform reflectivity CFADs that show larger peak modes in the convective CFADs, which is consistent with the results Steiner et al. (1995) used to verify their algorithm. CFADs for the Steiner and GCE methods are shown in Fig. 13a-d for PDA. At the lowest levels, the peak convective modes were close to 50 dBZ for GCE, C&H, CA20 and Xu down to 45 dBZ for Steiner and Vt-W for PDA. The stratiform modes range from 20 to 25 dBZ for GCE, C&H, CA20 and Xu to 20 dBZ for Steiner and 15 to 20 dBZ for Vt-W also for PDA. In addition, all of the stratiform CFADs from the PRESTORM case showed evidence both of a bright band and of decreasing magnitudes below the bright band indicative of evaporation. The effects of low-level evaporation are not seen in any of the convective CFADs. One distinct difference from the results of Steiner et al. (1995) is that most of the stratiform CFADs generated by the C-S techniques in this study are broader than those of the convective region. The Steiner and Vt-W methods are the exception.

Analysis of the reflectivity CFADs for the TOGA COARE case reveals similar trends to those from PRESTORM. Results from Steiner and GCE are shown in Fig. 13e-h for PDA. The GCE, C&H, and Xu methods are in close agreement all having convective peak modes just under 50 dBZ for both types of advection and peak stratiform modes near 20 dBZ for 4th order and near 30 dBZ for PDA. The CA20 method, however, is now a bit different. Though it still agrees with the others in terms of stratiform distribution peaks, it now has peak convective modes closer to 40 dBZ. Furthermore, the convective CFADs for the CA20 method are now much broader than those of GCE, C&H, and Xu. These results are likely attributable to the difference in cell structure between the PRESTORM and TOGA COARE cases. There were more numerous cells behind the leading edge in the TOGA COARE simulations. The Steiner method has smaller convective and stratiform peak modes than the first four methods, about 37 for the convective peaks and 18 and 25 dBZ for the 4th order and PDA stratiform peaks respectively. Finally, the Vt-W method shows the smallest convective peaks near 35 dBZ and fairly small stratiform peaks from 20 to 22 dBZ. Thus all the methods are again able to produce larger peak values for the convective region. All of the stratiform CFADs do show evidence of low-level

evaporation for the 4th order simulation, yet none of them show it for PDA. Only the CA20, Steiner and Vt-W methods show convective distributions that are close to being as broad as the stratiform distributions.

Vertical velocity CFADs for the PRESTORM case all have broader distributions in the convective region though the distributions are overall much narrower than those in Steiner et al. (1995). The vertical velocity CFADs for Vt-W and GCE for PDA are shown in Fig. 14a-d. At +5 m/s, the contour frequency is close to 1% at most levels in the current study whereas Steiner et al. (1995) has the frequency exceeding 10% at mid-levels. The reason for the discrepancy is that in the current study, clear areas, especially ahead of the leading edge above new convection, are counted as part of the convective region and skew the distributions closer to zero. Also, the horizontal domain in Steiner et al. (1995) is much smaller. The vertical velocity CFADs reveal that some of the separation techniques contain a few occurrences of strong vertical velocities in the stratiform region. These include a few 15 to 20 m/s updrafts in GCE, Xu, and CA20, and some that reach 25 to 30 m/s in C&H. The Steiner method has some 10 to 15 m/s updrafts in the stratiform region, while the Vt-W method contains no updrafts over 5 m/s in the stratiform region. These outliers are infrequent and do not affect the overall results, though they are clearly misclassified. Xu (1995), however, states that significant vertical velocities above the melting layer not associated with convective rain rates should be classified as stratiform as they are predominantly in the upper troposphere. The largest outliers do in fact occur about the freezing level, but they do not satisfy the condition $|w| \ll V_{ice}$ put forth by Houze (1993) and Steiner et al. (1995) where V_{ice} is of the order 1 to 3 m/s. The broadest convective and narrowest stratiform CFADs are those from Vt-W. Steiner is next, followed by the others which are similar to each other. The results are the same for both types of advection.

CFADs of vertical velocities for the TOGA COARE case, though slightly narrower, show similar characteristics compared to PRESTORM. Results for the GCE and Vt-W methods are shown in Fig. 14e-h for PDA. Convective CFADs for the 4th order run (not shown) do show an enhanced region of positive vertical velocities near 2 km compared to those for PDA. This may be a result of the more numerous shallow cells. Again, the Steiner and Vt-W methods have the broadest convective CFADs and the narrowest stratiform ones.

3.7 *Microphysical Processes*

In addition to the true CFADs of vertical velocity and radar reflectivity, another type of contoured diagram was made using microphysical data from the model. These diagrams, termed CDADs for Cumulative Distribution with Altitude Diagrams, were constructed by partitioning the microphysical processes of condensation, evaporation, deposition, sublimation, freezing and melting according to vertical velocity bins (the same used in the vertical velocity CFADs) again as a function of height, cumulatively. Finally, each bin was normalized by the total cumulative value for that process independent of the region (i.e., not convective or stratiform but total) involved so that the diagrams show as a function of W and Z the distribution of where a particular process occurs. These diagrams were constructed for the entire domain and for the convective and stratiform regions for each separation technique. Results for the entire domain are shown in Fig. 15. The total accumulated distributions of each the microphysical processes are also partitioned into convective and stratiform fractions for each separation technique. The results are listed in Tables 5, 6, 7, and 8.

In the PRESTORM simulations, the bulk of the condensation takes place in updrafts between 2 and up to 14 m/s between 1.5 and 6 km in altitude. All of the convective-stratiform separation techniques classify the bulk of the condensation as convective ranging from just over 70% for C&H in the 4th order run to over 97% for Steiner and Vt-W (see Tables 5&6). Based on the convective and stratiform CDADs (not shown), all of the methods show that evaporation can be separated into two rather distinct regimes. The first regime is the convective regime wherein evaporation occurs from the surface to up over 6 km with a significant portion from downdrafts stronger than -3 m/s. The convective distribution is skewed to the downdraft side extending to regions over -5 m/s. This evaporation is attributed to downdrafts along the periphery of rising updraft cores. The stratiform regime, on the otherhand, is narrower and confined below 4 km. The distribution is centered on the zero line and becomes even narrower near the surface. Evaporation in the stratiform region is dominated by rain falling beneath the anvil. Overall for the PRESTORM case, GCE, C&H, Xu and CA20 divide evaporation roughly equally between convective and stratiform.

Steiner and Vt-W place three-quarters of all evaporation in the convective region (Tables 5&6). The range being from 44% convective for C&H up to 81% for Vt-W inclusive of both advection types.

The results for deposition are more variable in the PRESTORM case. The total distribution lies mainly between 5 and 12 km and is skewed towards weaker updrafts though a significant portion extends past 10 m/s. The portion below about 5 m/s pertains to the stratiform region, while the convective portion of the distribution is centered between 5 and 7.5 m/s. This accounts for the shape of the overall distribution. The partitioning of deposition into convective and stratiform ranges from just over 30% convective for C&H in the PDA run to over 70% convective for Vt-W in the 4th order run. Overall, the methods treat deposition as half convective and half stratiform. There is a tendency for deposition to be more convective with 4th order advection. The difference is 10% on average. Sublimation predominantly occurs between 4 and 11 km in downdrafts of less than 5 m/s with the distribution skewed towards weaker downdrafts. Except for the Steiner and Vt-W methods, 75-80% of sublimation is stratiform. Steiner and Vt-W are slightly lower between 60 and 70%.

Freezing is treated as a convective process by all of the convective-stratiform techniques. It is almost completely convective (over 96%) in Steiner and Vt-W and strongly convective in the rest with C&H the lowest at 65% for 4th order. The distribution is slightly different between 4th order and PDA. The distribution extends from the freezing level near 4 km up to 9 km. The difference between the 4th order (not shown) and PDA distributions comes from the contribution by stronger updrafts. For updrafts over 7-8 m/s, most of the freezing occurs within a kilometer of the freezing level in PDA whereas it's spread more uniformly over 3 to 4 km with 4th order advection. The results vary in the assessment of melting. In C&H, melting is nearly half convective while in Steiner and Vt-W it is over 80% convective. Convective melting has a wider distribution from -10 to 10 m/s while melting in the stratiform region is confined between -5 and 4 m/s. The stratiform distribution peaks near 0 m/s while the convective distribution is spread from 0 to -5 m/s. Overall, most of the melting falls into the convective category though a significant portion occurs in the stratiform region.

With TOGA COARE, the results for condensation are similar in terms of the partitioning but differ in terms of distribution. Again, condensation is found to be predominantly convective. Vt-W and Steiner are the most convective (up to 92% for Vt-W in the 4th order run). The C&H method considers only 55% of the condensation to be convective in the PDA run. In general, the percentage of condensation that is found to be convective is at least 10% lower per method compared to the PRESTORM case. The distribution differs significantly from the PRESTORM results. Condensation has two peaks at lower levels that merge into a single peak at mid-levels. This structure is similar for both 4th order and PDA. The convective distributions show an ascending axis that extends from 10 m/s at 2 km up to 1 m/s at 4 km. The stratiform portion of the condensation distribution is narrow and lies along the zero axis below 2 km. It widens above 2 km and extends all the way up to 8 km with a peak just above 4 km at 1 m/s. The separation methods produce consistent convective and stratiform patterns of condensation as functions of height and updraft. There is considerable variation in the partitioning of evaporation between the methods. The GCE, C&H, and Xu methods lean heavily towards the stratiform side with percentages over 70% stratiform. Steiner and Vt-W are slightly convective with percentages around 55% convective. CA20 falls in between with near 40% convective. The distributions for the convective, stratiform and total regions are similar. Evaporation extends from the surface up to 6 or 8 km (slightly higher for stratiform). It is centered on 0 m/s and falls between 3 m/s with the stratiform distribution slightly narrower. Again, the structures are similar among the various methods.

As in the PRESTORM case, the characterization of deposition as being either convective or stratiform varies widely among the separation methods. The differences for TOGA COARE are even larger with C&H having as little as 3.7% convective (PDA) and Vt-W up to 67.5% convective (PDA). The distribution lies mostly between 5 and 13 km and is skewed towards zero with significant values below 8-9 m/s. Among the methods that have a meaningful convective amount, the convective side is broader while the stratiform portion is taller and narrower. Sublimation likewise shows a tremendous variation in its convective/stratiform designation varying from 2.6% convective (C&H) to 48.5% (Vt-W). The distribution is centered on zero m/s and varies between 5 m/s.

Unlike PRESTORM, freezing is no longer predominantly convective. The variation is now considerable between the methods. The most significant changes occurred with the C&H and GCE methods. With the GCE method, the convective freezing portion drops from 80.1% in PRESTORM (4th) to 24% in TOGA COARE (4th). Similarly C&H dropped from 65 to 12.6% (both 4th order values). Freezing is still over 90% convective in Vt-W (PDA). The total distribution begins with a very broad base just above the freezing level attributed to the convective region. The convective portion is rather shallow, however, so that the upper part of the distribution stems from the stratiform region and leans toward weaker updrafts with height. Another big change between the PRESTORM and TOGA COARE cases involves the melting. All of the techniques agree in substantially lowering the percentage of convective melting in the TOGA COARE case down just over 3% for C&H (4th) to 61% for Vt-W (PDA). The greatest reduction occurs in the C&H, GCE, Xu and CA20 methods and is on the order of 40% or more. Steiner and Vt-W are also noticeably reduced, near 35% and 20 to 30% respectively. This shifts melting from more of a convective process in PRESTORM to a stratiform one in TOGA COARE. The distribution of melting is more confined in TOGA COARE compared to PRESTORM with respect to updraft and vertical extent. Melting occurs within 1.5 km of the melting level. In the 4th order run, the distribution is centered on 0 m/s and spans 5 m/s. The PDA run shows a tail up to 10 m/s that comes from the convective region.

3.8 *Latent Heating Retrieval*

One of the major objectives in the current use of convective-stratiform separation is the retrieval of latent heating profiles from observed rainfall data by using numerical cloud model data as a proxy for the cloud systems in the real environment (Tao et al. 1990; 1993; 2000). The Goddard Convective-Stratiform Heating algorithm (Tao et al. 1990; 1993; 2000) retrieves latent heating profiles for observed convective systems by using observed rainfall as a multiplier and observed stratiform amount as a weighting factor on appropriate rainfall-normalized convective and stratiform heating profiles. The technique takes advantage of the characteristic shapes in the vertical of the latent heating in the convective and stratiform regions of mesoscale convective systems. Tao et al.

(1993a) stated that the stratiform percentage needed to be accurate to within 10% for an accurate retrieval. This is based on the fact that the level of maximum heating shifts upward with increasing stratiform fraction and 10% accuracy is sufficient to define the peak level.

The sensitivity of the retrieved heating profiles to the choice of separation technique can also be tested and is shown in Fig. 16 for the PRESTORM and TOGA COARE PDA cases. Treating the model simulations as substitutes for the real system and using the observed stratiform amount of 29% (Johnson and Hamilton 1988) for the PRESTORM case, sample retrieved profiles are produced following the CSH retrieval algorithm for this case. The results show that all of the retrieved profiles are more stratiform in appearance than what the true heating profile in the model is although the GCE, C&H, CA20 and Xu based profiles are very good approximations. The Vt-W and Steiner based profiles actually shift the peak heating level too high compared to the other four which have their peak heating level the same as the true profile. Of course, the closer a particular method was in the simulation to the chosen stratiform percentage of 29%, the better its chance would be of matching the true model heating. This is consistent with the results seen and is the same for both types of advection. Applying this same sensitivity test to the TOGA COARE case using the model results and an observed value of 40% stratiform (Short et al. 1997), the GCE, C&H, and Xu profiles are actually able reproduce the true model heating. The CA20 and Vt-W profiles are a little too stratiform in their appearance while Steiner again produces an exaggerated stratiform bias. The GCE, C&H, and Xu methods were of course closer in their estimated stratiform percentage to the chosen observed value of 40%. This does not necessarily mean that the others are going to produce poor retrievals. Even though two different separation methods may yield significantly different stratiform percentages, it is the rain normalized profiles that matter. So a method with large stratiform heating aloft and cooling below and a large stratiform rain amount can have the same rain normalized profile as a method with much smaller anvil heating and cooling if the proportion of heating and cooling to surface rainfall in the anvil is the same for different sized areas. As evidenced by the convective and stratiform rain-normalized heating profiles in Fig. 17, this is clearly not the case for all six methods. While the convective profiles for the PRESTORM case do show a lot of uniformity, the stratiform profiles do not. Specifically, the Vt-W and even

more so the Steiner stratiform profiles significantly diverge from the other stratiform profiles. Their shapes appear amplified with respect to the others. This is a direct result of having small stratiform rain amounts by which to normalize by in combination with significant heating and cooling present in the simulated anvil region with little or no associated surface precipitation. This can have a large impact on the retrieved profiles. The TOGA COARE profiles also show stratiform profiles that appear to be amplified relative to the rest. This time the CA20 and Steiner profiles are involved. The Vt-W profiles, however, show that there can also be fundamental changes in the basic shapes not related to just division by a smaller denominator.

4.0 Summary and Conclusions

Six different convective-stratiform separation techniques were compared and evaluated using 2D numerical simulations of a tropical (TOGA COARE) and midlatitude continental (PRESTORM) squall line. The six techniques included in the study were based on: Churchill and Houze (1984), Tao et al. (1993b), Xu (1995), a simple Constant Area (e.g. Caniaux 1994), Steiner et al. (1995), and a new Vt-W method based on the premise that the terminal velocity of hydrometeors is large relative to air velocity in stratiform precipitation (Houghton 1968; Steiner et al. 1995; Houze 1997). The simulations were made using two different numerical advection schemes: 4th order and PDA. The overall objective was to assess the sensitivity of partitioned quantities such as rainfall, mass flux, Q1, Q2, microphysics and latent heating retrieval to the use of different convective-separation techniques and to determine the effects of the numerical advection schemes on the simulated systems.

In terms of rainfall, it was found that overall rainfall was not significantly effected (less than 2%) by the numerical advection for either case. However, estimated stratiform percentages varied significantly among the separation techniques: from 4 to 22% in PRESTORM and 12 to 49% in TOGA COARE. The C&H and GCE methods tended to produce the highest stratiform portion and Steiner and Vt-W the lowest. Johnson and Hamilton (1988) reported a stratiform rain amount of 29% for the PRESTORM case using gauge data making all of the techniques appear too low in the model. However, applying the convective rainrate threshold used by Johnson and Hamilton (1988) in the model results in

a stratiform portion of just 4% (PDA) which agrees quite well with the lowest estimate given by Steiner. Even though the gauge threshold may not be expected to yield the same percentage in the model, this indicates the model likely underestimates the frequency of light rainrates as was found by Sui et al. (1998) making it difficult to evaluate the performance of individual methods based on comparison the observed percentage. Short et al. (1997) reported that 40% of the rainfall that occurred during active periods in TOGA COARE was stratiform in good agreement with the C&H, GCE and Xu methods in the model. The same caveats would apply however. All of the separation techniques were consistent in finding larger stratiform amounts in the tropical case.

Storm structure was found to be invariant with respect to advection scheme in the PRESTORM case, but not so with the TOGA COARE case. More numerous shallow cells are produced along the leading edge of the squall system using 4th order advection while PDA leads to fewer deeper cells that persist longer behind the leading edge resulting in more cells embedded within the stratiform region. This in turn leads to more variation between the separation techniques.

The average convective width, including the coherence approach, was found to be 95 km for PDA in the PRESTORM case and 27 km in TOGA COARE. These are very close to the mean CA20 values of 91 and 28 km respectively suggesting that the assumed characteristic convective width of 20 km in the CA20 method was a reasonable approximation.

Positive definite advection slightly increased the mean cloud coverage for both the PRESTORM and TOGA COARE cases. In addition, average cloudtop was a kilometer higher in the PDA run for TOGA COARE due to the taller cells.

Total mass flux profiles for both types of advection were nearly identical at all levels in the PRESTORM case but differed in the TOGA COARE case. The TOGA COARE PDA profile had more upward motion aloft in association with the taller penetrating cells while the 4th order profile had more net upward mass flux between 2 and 6 km. The convective and stratiform mass flux profiles for the six separation techniques in the PRESTORM case had similar characteristic shapes. The level of peak upward mass flux varied a great deal in the convective

region (from 3.5 to 6.5 km for PDA) with less variation in the height of the anvil peak (between 8 and 10 km). In the TOGA COARE case, the separation techniques showed much less variation at low levels where the convective profiles all peaked near 2.5 km (PDA). Differences mainly occurred above 4 km due to the lack of significant vertical motion at low levels behind the leading edge. C&H, GCE, and CA20 assigned nearly all of the net upward mass fluxes aloft to the stratiform region while increasingly Xu, Steiner and Vt-W assigned them to the convective region significantly altering the shape of the profiles. Thus qualitatively the separation techniques were found to agree but differ significantly in terms of magnitude.

As with mass flux, apparent heating was found to be independent of advection for the PRESTORM case but not so for TOGA COARE. Again as a result of the difference in cell structure, total heating was larger above 10 km in the PDA simulation while 4th order heating was greater at lower levels (2-6 km). Again, qualitatively the separation techniques agree in terms of convective and stratiform Q1 profiles. Below 4 km in PRESTORM, the profiles agree quite closely with one another. The largest differences occur at mid-levels where peak convective heating ranges from 0.43 to 0.75 (deg/mm) for PDA. Below 4 km, the variation among the methods is also very small in the TOGA COARE case. Aloft, C&H, GCE, and CA20 similarly assign the bulk of the heating to the stratiform region while increasingly in order Xu, Steiner and Vt/W assign more to the convective region resulting in an overall range of 0.2 to 0.63 (deg/mm) of peak anvil heating at 9 km. Overall the midlatitude convective heating profiles peak at a higher level and heating occurs over a much broader layer compared to the tropical profiles. In the anvil, low-level cooling is deeper and more pronounced in the tropical profiles while latent heating aloft is greater.

The apparent moistening (Q2) profiles for the two PRESTORM runs are nearly the same. The pattern is very similar with the TOGA COARE results except that convective drying is a little stronger for the 4th order simulation and hence the total profile as well. The variation among the convective and anvil Q2 profiles is somewhat larger in the PRESTORM runs than in the TOGA COARE runs where the variation is quite small. The CA20 profiles have the largest convective drying and anvil moistening in the PRESTORM case and account for the larger variation. The deeper cells in the TOGA COARE PDA run

do allow for some variation above 4 km where the Vt-W method shows the widest separation between convective drying and anvil moistening. Again all the methods show a qualitative consensus.

Despite the fact the GCE method is the only one that directly uses hydrometeor information to differentiate between convective and stratiform areas, the amount of convective cloud water or cloud ice for the GCE method relative to the others followed the overall rank in convective-stratiform separation. All of the methods found the bulk of cloud water to be convective in the PRESTORM case. The results for cloud ice were split ranging from nearly equal parts convective and anvil with C&H to over 80% convective with Vt/W. For TOGA COARE, the variation in the amount of convective cloud water was large while nearly all the methods expect for Steiner and Vt-W had cloud ice as overwhelmingly stratiform.

Contoured Frequency with Altitude Diagrams (CFADs) were constructed for both the PRESTORM and TOGA COARE cases for each of the various separation algorithms. The PRESTORM reflectivity CFADs for each of the separation algorithms did indeed have larger peak modes in their convective CFADs. They also all had stratiform CFADs that showed evidence of a bright band. However, only Steiner and Vt-W had convective CFADs that were broader than their stratiform ones. The trends were similar for the TOGA COARE case except that the CA20 method produced somewhat broader convective CFADs and the stratiform CFADs for the PDA run did not show evidence of low-level evaporation. Vertical velocity CFADs for the PRESTORM case show that all of the methods have broader distributions in the convective region. The stratiform CFADs did show instances where points were clearly misclassified. CFADs of vertical velocities for the TOGA COARE case show similar behavior. Just as with PRESTORM, Vt-W produces the narrowest stratiform vertical velocity CFADs followed by Xu and Steiner. Thus all of the methods are able to satisfy the condition of having larger convective peak frequencies but not necessarily distributions that are broader for the convective regime.

Modified CFADs were constructed on the microphysical processes in the model to show how the processes were distributed as a function of W and Z .

Most of the microphysical processes were distributed over a wider velocity and vertical range in the midlatitude case. The processes were also partitioned into convective and stratiform portions for each method. Condensation varied from 98 (Steiner and Vt/W) to 71% (C&H) convective in the PRESTORM case and 92 (Vt/W) to 55% (C&H) convective in TOGA COARE. Evaporation pretty evenly split between convective and stratiform in PRESTORM and was mainly stratiform in TOGA COARE. Deposition varied greatly ranging from 70 (Vt/W) to 31% (C&H) convective in PRESTORM to between 68 (Vt/W) and 4% (C&H) in TOGA COARE. Sublimation was clearly stratiform though Steiner and Vt/W divided it nearly evenly in TOGA COARE. Freezing was strongly convective in PRESTORM but varied considerably in TOGA COARE from 13% (C&H) to 92% (Vt/W) convective. Melting mainly occurred in the convective region in PRESTORM while the opposite was true for TOGA COARE. The values are inclusive of both forms of advection. Thus depending on the process, the methods varied widely in their characterization and more so in the tropical case.

Latent heating retrieval was shown to be quite sensitive to the use of separation technique. This was mainly attributed to the stratiform region especially for methods that found very little stratiform rain (i.e., Steiner and Vt/W).

Overall, it was found that the different separation techniques produced results that qualitatively agreed. However, the quantitative differences were significant. Observational comparisons were unable to conclusively evaluate the performance of the techniques. Thus it is important when using various convective-stratiform separation the sensitivities involved. Although not addressed in this study, it may be useful to add an additional category in the separation of convective systems: the transition region. Indeed, some of the differences between the methods studied here are related to their treatment of the transition area. C&H would be the most likely method to treat it as stratiform and Vt/W the most likely to treat it as convective. As cells move from the leading edge of the system rearward, it can be very arbitrary when to change their designation from convective to stratiform. As such, based on the fact that many of the separation techniques look for convective criteria only below the melting level, it may be useful in the future to define the convective region as that where convective criteria are exceeded below the melting level, the

transition region as that where convective criteria are only exceeded above the melting level, and the remaining region as stratiform.

5. Acknowledgments

This work is supported by the NASA Headquarters Atmospheric Dynamics and Thermodynamics Program and by the NASA TRMM project. These authors are grateful to Dr. R. Kakar (NASA/HQ) for his support of this research and to Dr. W. Olson for providing the code for the Steiner et al. (1995) separation technique. Acknowledgment is also made to NASA/ Goddard Space Flight Center for computer time used in the research.

6. References

- Adler, R.F., and A.J. Negri, 1988: A satellite infrared technique to estimate tropical convective and stratiform rainfall. *J. Appl. Meteor.*, **27**, 30-51.
- Alexander, G.D., and W.R. Cotton, 1998: The use of cloud-resolving simulations of mesoscale convective systems to build a mesoscale parameterization scheme. *J. Atmos. Sci.*, **55**, 2137-2161.
- Atlas, D., Ed., 1990: Radar in meteorology. *American Meteorological Society*, 806 pp.
- Battan, L.J., 1973: Radar observation of the atmosphere. *The University of Chicago Press*, 161 pp.
- Brown, R.M., 1979: Mesoscale unsaturated downdrafts driven by rainfall evaporation: A numerical study. *J. Atmos. Sci.*, **36**, 313-335.
- Byers, H.R., and R.R. Braham Jr., 1949: The Thunderstorm. *U.S. Government Printing Office*, 287 pp.
- Caniaux, G., J.-L. Redelsperger, and J.-P. Lafore, 1994: A numerical study of the stratiform region of a fast-moving squall line. Part I: General description and water and heat budgets. *J. Atmos. Sci.*, **51**, 2046-2074.
- Chin, H.-N. S., 1994: The impact of the ice phase and radiation on a mid-latitude squall line system. *J. Atmos. Sci.*, **51**, 3320-3343.
- Churchill, D.D., and R.A. Houze Jr., 1984: Development and structure of winter monsoon cloud clusters on 10 December 1978. *J. Atmos. Sci.*, **41**, 933-960.
- Fairall, C.W., E.F. Bradley, D.P. Rogers, J.B. Edson, and G.S. Young, 1996: Bulk parameterization of air-sea fluxes for Tropical Ocean Global Atmosphere Coupled Ocean-Atmosphere Response Experiment. *J. Geophys. Res.*, **101**, 915-929.

- Ferrier, B.S., S. Simpson, and W.-K. Tao, 1996: Factors responsible for different precipitation efficiencies between midlatitude and tropical squall simulations. *Mon. Wea. Rev.*, **124**, 2100-2125.
- Frank, W.M., and J.L.M. McBride, 1989: The vertical distribution of heating in AMEX and GATE cloud clusters. *J. Atmos. Sci.*, **46**, 3464-3478.
- Gamache, J.F., and R.A. Houze Jr., 1982: Mesoscale air motions associated with a tropical squall line. *Mon. Wea. Rev.*, **110**, 118-135.
- Hamilton, R.A., and J.W. Archbold, 1945: Meteorology of Nigeria and adjacent territory. *Quart. J. Roy. Meteor. Soc.*, **71**, 231-262.
- Houghton, H. G., 1968: On precipitation mechanisms and their artificial modification. *J. Appl. Meteor.*, **7**, 851-859.
- Houze, R.A., Jr., 1973: A climatological study of vertical transports by cumulus-scale convection. *J. Atmos. Sci.*, **30**, 1112-1123.
- Houze, R.A., Jr., 1977: Structure and dynamics of a tropical squall-line system. *Mon. Wea. Rev.*, **105**, 1540-1567.
- Houze, R.A., Jr., 1982: Cloud clusters and large-scale vertical motions in the tropics. *J. Meteor. Soc. Japan*, **60**, 396-410.
- Houze, R.A., Jr., 1993: *Cloud Dynamics*. Academic Press, 573 pp.
- Houze, R.A., Jr., 1997: Stratiform precipitation in regions of convection: a meteorological paradox? *Bull. Amer. Met. Soc.*, **78**, 2179-2196.
- Johnson, D., W.-K. Tao, J. Simpson, and C.-H. Sui, 2000: A study of the response of deep tropical clouds to mesoscale processes, Part I: Modeling strategy and simulation of TOGA COARE convective systems, *J. Atmos. Sci.*. (submitted).
- Johnson, R.H., 1984: Partitioning tropical heat and moisture budgets into cumulus and mesoscale components: Implications for cumulus

- parameterization. *Mon. Wea. Rev.*, **112**, 1590-1601.
- Johnson, R.H., and P.J. Hamilton, 1988: The relationship of surface pressure features to the precipitation and airflow structure of an intense midlatitude squall line. *Mon. Wea. Rev.*, **116**, 1444-1472.
- Johnson, R.H., and G.S. Young, 1983: Heat and moisture budgets of tropical mesoscale anvil clouds. *J. Atmos. Sci.*, **40**, 2138-2147.
- Jorgensen, D.P., M.A. LeMone, and S.B. Trier, 1997: Structure and evolution of the 22 February 1993 TOGA-COARE squall line: Observations of precipitation, circulation, and surface energy fluxes. *J. Atmos. Sci.*, **54**, 1961-1985.
- Leary, C.A., and R.A. Houze Jr., 1979: Melting and evaporation of hydrometeors in precipitation from the anvil clouds of deep tropical convection. *J. Atmos. Sci.*, **36**, 669-679.
- LeMone, M.A., D.P. Jorgensen, and B.F. Smull, 1994: The impact of two convective systems of sea surface stresses in COARE. *Preprints, 6th Conference on Mesoscale Processes*, Amer. Meteor. Soc., Portland, 40-44.
- Lin, Y.-L., R.D. Farley and H.D. Orville, 1983: Bulk parameterization of the snow field in a cloud model. *J. Clim. Appl. Meteor.*, **22**, 1065-1092.
- Newton, C.W., 1950: Structure and mechanism of the prefrontal squall line. *J. of Meteor.*, **7**, 210-222.
- Redelsperger, J.-L., P.R.A. Brown, F. Guichard, C. Hoff, M. Kawasima, S. Lang, Th. Montmerle, K. Nakamura, K. Saito, C. Seman, W.-K. Tao, and L.J. Donner, 2000: A GCSM model intercomparison for a tropical squall line observed during TOGA-COARE. Part I: Cloud-resolving models. *Quart. J. Roy. Meteor. Soc.*, **126**, 823-863.
- Reed, R.J., and E.E. Recker, 1971: Structure and properties of synoptic-scale wave disturbances in the equatorial western pacific. *J. Atmos. Sci.*, **28**, 1117-1133.

- Rutledge, S.A., and P.V. Hobbs, 1984: The mesoscale and microscale structure and organization of clouds and precipitation in midlatitude clouds. Part XII: A diagnostic modeling study of precipitation development in narrow cold frontal rainbands. *J. Atmos. Sci.*, **41**, 2949-2972.
- Rutledge, S.A., R.A. Houze Jr., M.I. Biggerstaff, and T. Matejka, 1988: The Oklahoma-Kansas mesoscale convective system of 10-11 June 1985: Precipitation structure and single-doppler radar analysis. *Mon. Wea. Rev.*, **116**, 1409-1430.
- Ryde, J.W., 1946: The attenuation and radar echoes produced at centimeter wavelengths by various meteorological phenomena. *Meteorological Factors in Radio Wave Propagation*, Physical Society, London, 169-188.
- Short, D.A., P.A. Kucera, B.S. Ferrier, J.C. Gerlack, S.A. Rutledge, and O.W. Thiele, 1997: Shipboard Radar Rainfall Patterns within the TOGA COARE IFA. *Bull. Amer. Met. Soc.*, **78**, 2817-2836.
- Simpson, J., 1980: Downdrafts as linkages in dynamic cumulus seeding effects. *J. Appl. Meteor.*, **19**, 477-487.
- Simpson, J., R. Adler, and G. North, 1988: A proposed tropical rainfall measuring mission (TRMM) satellite. *Bull. Amer. Met. Soc.*, **69**, 278-295.
- Simpson, J., and W.-K. Tao, 1993: Goddard Cumulus Ensemble Model. Part II: Applications for studying cloud precipitating processes and for NASA TRMM. *Terrestrial, Atmospheric and Oceanic Sciences*, **4**, 73-116.
- Smolarkiewicz, P.K., 1983: A simple positive definite advection scheme with small implicit diffusion. *Mon. Wea. Rev.*, **111**, 479-486.
- Smolarkiewicz, P.K., 1984: A fully multidimensional positive definite advection transport algorithm with small implicit diffusion. *J. Comput. Phys.*, **54**, 325-362.
- Smolarkiewicz, P.K., and W.W. Grabowski, 1990: The multidimensional

- positive advection transport algorithm: nonoscillatory option. *J. Comput. Phys.*, **86**, 355-375.
- Soong, S.-T., and Y. Ogura, 1973: A comparison between axisymmetric and slab symmetric cumulus models. *J. Atmos. Sci.*, **30**, 879-893.
- Steiner, M., R.A. Houze Jr., and S.E. Yuter, 1995: Climatological characterization of three-dimensional storm structure from operational radar and rain gauge data. *J. Appl. Meteor.*, **34**, 1978-2007.
- Sui, C.-H., X. Li, and K.-M. Lau, 1998: Radiative-convective processes in simulated diurnal variations of tropical oceanic convection. *J. Atmos. Sci.*, **55**, 2345-2357.
- Tao, W.-K., and J. Simpson, 1984: Cloud interactions and merging: numerical simulations. *J. Atmos. Sci.*, **41**, 2901-2917.
- Tao, W.-K., and S.-T. Soong, 1986: A study of the response of deep tropical clouds to mesoscale processes: Three-dimensional numerical experiments. *J. Atmos. Sci.*, **43**, 2653-2676.
- Tao, W.-K., and J. Simpson, 1989: Modeling study of a tropical squall-type convective line. *J. Atmos. Sci.*, **46**, 177-202.
- Tao, W.-K., and J. Simpson, 1993: Goddard Cumulus Ensemble Model. Part I: Model description. *Terrestrial, Atmospheric and Oceanic Sciences*, **4**, 35-72.
- Tao, W.-K., S. Lang, J. Simpson, and R. Adler, 1993a: Retrieval algorithms for estimating the vertical profiles of latent heat release: Their applications for TRMM. *J. Meteor. Soc. Japan*, **71**, 685-700.
- Tao, W.-K., J. Simpson, C.-H. Sui, B. Ferrier, S. Lang, J. Scala, M.-D. Chou, and K. Pickering, 1993b: Heating, moisture, and water budgets of tropical and midlatitude squall lines: Comparisons and sensitivity to longwave radiation. *J. Atmos. Sci.*, **50**, 673-690.

- Tao, W.-K., S. Lang, J. Simpson, C.-H. Sui, B. Ferrier, and M.-D. Chou, 1996: Mechanisms of cloud-radiation interaction in the tropics and midlatitudes. *J. Atmos. Sci.*, **53**, 2624-2651.
- Tao, W.-K., S. Lang, J. Simpson, W.S. Olson, D. Johnson, B. Ferrier, C. Kummerow, and R. Adler, 2000: Vertical profiles of latent heat release and their retrieval for TOGA COARE convective systems using a cloud resolving model, SSM/I, and ship-borne radar data. *J. Meteor. Soc. Japan*, **78**, 333-355.
- Trier, S.B., W.C. Skamarock, M.A. LeMone, D.B. Parsons, and D.P. Jorgensen, 1996: Structure and evolution of the 22 February 1993 TOGA-COARE squall line: numerical simulations. *J. Atmos. Sci.*, **53**, 2861-2886.
- Trier, S.B., W.C. Skamarock, and M.A. LeMone, 1997: Structure and evolution of the 22 February 1993 TOGA-COARE squall line: Organization mechanisms inferred from numerical simulation. *J. Atmos. Sci.*, **54**, 386-407.
- Wang, Y., W.-K. Tao, and J. Simpson, 1996: The impact of a surface layer on a TOGA COARE cloud system development. *Mon. Wea. Rev.*, **124**, 2753-2763.
- Wang, Y., W.-K. Tao, J. Simpson, and S. Lang, 2000: The sensitivity of tropical squall lines to surface fluxes: cloud resolving model simulations. *Quart. J. Roy. Meteor. Soc.*, (submitted)
- Wescott, N., 1984: A historical perspective on cloud mergers. *Bull. Amer. Meteor. Soc.*, **65**, 219-226.
- Xu, K.-W., 1995: Partitioning mass, heat, and moisture budgets of explicitly simulated cumulus ensembles into convective and stratiform components. *J. Atmos. Sci.*, **52**, 1-23.
- Yanai, M., S. Esbensen, and J.-H. Chu, 1973: Determination of bulk properties of tropical cloud clusters from large-scale heat and moisture budgets. *J. Atmos. Sci.*, **30**, 611-627.
- Yuter, S.E. and R.A. Houze Jr., 1995b: Three-dimensional kinematic and micro-

physical evolution of Florida cumulonimbus. Part II: Frequency distributions of vertical velocity, reflectivity, and differential reflectivity. *Mon. Wea. Rev.*, **123**, 1941-1963.

Zipser, E.J., 1977: Mesoscale and convective-scale downdrafts as distinct components of squall-line structure. *Mon. Wea. Rev.*, **105**, 1568-1589.

TABLES

- Table 1 Characteristics of the large scale environments associated with the PRESTORM and TOGA COARE squall line cases. Simulation domain size and grid spacing and references are also listed.
- Table 2 Main criteria used by the six different separation algorithms to partition convective and stratiform regions.
- Table 3 Total accumulated rainfall (mm) per grid point over all 12 hours of simulation time for all four PRESTORM and TOGA COARE simulations. Mean stratiform percentages for all six convective-stratiform separation techniques are also shown for each simulation. Values in parentheses are for the last 4 hours of simulation time.
- Table 4 Mean width (km) of the convective and stratiform regions over 12 hours of simulation for all six separation methods and their average for all four simulations.
- Table 5 Total mean percentage of the microphysical processes that are convective according to each separation technique for the PRESTORM simulation with 4th order advection.
- Table 6 Total mean percentage of the microphysical processes that are convective according to each separation technique for the PRESTORM simulation with PDA.
- Table 7 Total mean percentage of the microphysical processes that are convective according to each separation technique for the TOGA COARE simulation with 4th order advection.
- Table 8 Total mean percentage of the microphysical processes that are convective according to each separation technique for the TOGA COARE simulation with PDA.

FIGURE CAPTIONS

- Fig. 1. Vertical cross-sections of model estimated radar reflectivity (dBZ) after 720 minutes of simulation for **(a)** the PRESTORM case with 4th order advection, **(b)** the PRESTORM case with PDA, **(c)** the TOGA COARE case with 4th order advection, and **(d)** the TOGA COARE case with PDA. The convective regions for each of the separation techniques are overlaid in solid black lines. Traces of the corresponding surface rainrates (mm/h) are also overlaid (top of the domain = 200 mm/h).
- Fig. 2. Time-domain cross-sections of surface rainfall rates (mm/h) for **(a)** the PRESTORM case with 4th order advection, **(b)** the PRESTORM case with PDA, **(c)** the TOGA COARE case with 4th order advection, and **(d)** the TOGA COARE case with PDA.
- Fig. 3. Time series of instantaneous grid averaged total (solid) and stratiform (dashed) rainrate for both types of advection for the **(a)** PRESTORM and **(b)** TOGA COARE cases.
- Fig. 4. Vertical profiles of mean cloud coverage as a percentage of the horizontal domain for both types of advection for both the PRESTORM and TOGA COARE cases.
- Fig. 5. Vertical profiles of domain average accumulated mass flux for the total (heavy dash), convective (solid) and stratiform (dotted) regions for both types of advection for the **(a)** PRESTORM and **(b)** TOGA COARE cases.
- Fig. 6. Vertical profiles of domain average accumulated convective and stratiform mass flux for each of the six separation techniques using PDA for the **(a)** PRESTORM and **(b)** TOGA COARE cases. [C&H - black dashed, GCE - solid black, Xu - gray dotted, CA20 - solid gray, Steiner - black dotted, Vt-W - "#"]
- Fig. 7. Vertical profiles of rain normalized domain average apparent heating (Q_1) for the total (heavy dash), convective (solid) and stratiform (dotted) regions for both types of advection for the **(a)** PRESTORM and **(b)** TOGA

COARE cases.

- Fig. 8. Vertical profiles of rain normalized Q1 components for the (a) PRESTORM convective region, (b) PRESTORM anvil region, (c) TOGA COARE convective region, and (d) TOGA COARE anvil region for PDA. [Condensation - solid, Deposition - thin solid, Evaporation - dotted, Sublimation - thin dotted, Freezing/Melting - thick dashed, Eddy flux - "e", Radiation - "+"]
- Fig. 9. Vertical profiles of rain normalized domain average convective and stratiform Q1 for each of the six separation techniques for (a) the PRESTORM case with 4th order advection, (b) the PRESTORM case with PDA, (c) the TOGA COARE case with 4th order advection, and (d) the TOGA COARE case with PDA. Line patterns follow Fig. 6.
- Fig. 10. Vertical profiles of rain normalized domain average apparent moistening (Q2) for the total (heavy dash), convective (solid) and stratiform (dotted) regions for both types of advection for the (a) PRESTORM and (b) TOGA COARE cases.
- Fig. 11. Vertical profiles of rain normalized domain average convective and stratiform Q2 for each of the six separation techniques for (a) the PRESTORM case with 4th order advection, (b) the PRESTORM case with PDA, (c) the TOGA COARE case with 4th order advection, and (d) the TOGA COARE case with PDA. Line patterns follow Fig. 6.
- Fig. 12. Vertical profiles of domain average hydrometeor content for (a) the PRESTORM case with 4th order advection, (b) the PRESTORM case with PDA, (c) the TOGA COARE case with 4th order advection, and (d) the TOGA COARE case with PDA. [Rain - solid black, Cloud - dotted black, Snow - solid gray, Cloud ice - dotted gray, Hail - thick dashed black, Graupel - thick dashed gray]
- Fig. 13. Reflectivity CFADs for the (a) PRESTORM convective region using GCE separation, (b) PRESTORM anvil region using GCE separation, (c) PRESTORM convective region using Steiner separation, (d) PRESTORM

anvil region using Steiner separation, (e) TOGA COARE convective region using GCE separation, (f) TOGA COARE anvil region using GCE separation, (g) TOGA COARE convective region using Steiner separation, (h) TOGA COARE anvil region using Steiner separation for PDA.

Fig. 14. Same as Fig. 13 except for vertical velocity and Vt-W separation in place of Steiner.

Fig. 15. Domain total microphysical CDADs of (a) PRESTORM condensation, (b) PRESTORM evaporation, (c) PRESTORM deposition, (d) PRESTORM sublimation, (e) PRESTORM freezing, (f) PRESTORM melting, (g) TOGA COARE condensation, (h) TOGA COARE evaporation, (i) TOGA COARE deposition, (j) TOGA COARE sublimation, (k) TOGA COARE freezing, (l) TOGA COARE melting,

Fig. 16. Simulated profiles of retrieved heating (Q_1) for each of the six separation techniques applied to model data (PDA) but using observed stratiform percentages for (a) PRESTORM and (b) TOGA COARE. The actual model heating is shown by the thick solid black line. Line patterns follow Fig. 6.

Fig. 17. Convective and stratiform heating profiles normalized by their respective rainfall amounts for each of the six separation techniques for the (a) PRESTORM convective region, (b) PRESTORM anvil region, (c) TOGA COARE convective region, and (d) TOGA COARE anvil region.

Table 1

	CAPE $m^2 s^{-2}$	Lifted Index	Precipitable Water ($g\ cm^{-2}$)	Richardson Number	$\Delta x, \Delta z$ (m) (Lx, Lz) (km)	References
TOGA COARE	1776	-3.20	6.334	74	750, 40-1100 (1906, 22)	Wang <i>et al.</i> 1996
PRESTORM	2300	-5.37	4.282	25	1000, 225-1000 (2543, 20)	Tao <i>et al.</i> 1993, 1996

Table 2

Method	Main Input
GCE Model	Surface Rainfall and Its Gradient, W and RH aloft
Churchill & Houze	Surface Rainfall and its Gradient
Xu (UCLA-CSU)	W and its Gradient below melting level
Constant Area	Maximum Rainfall location, Convective width
Steiner et al	Radar Reflectivity and its Gradient below melting level
V _T -W	W and terminal velocity

Table 3

	TOGA		PRESTORM	
	4th	PDA	4th	PDA
Rainfall	5.8	5.7	10.8	10.6
	Stratiform (%)		Stratiform (%)	
GCE	37	45 (53)	17	18 (30)
C&H	42	49 (56)	20	22 (32)
Xu	35	42 (55)	13	13 (23)
CA (20 km)	27	33 (42)	18	18 (28)
Steiner	12	17 (24)	5	4 (6)
Vt-W	16	19 (30)	5	6 (11)

Table 4

	PRESTORM		TOGA	
	4th	PDA	4th	PDA
	Convective/Stratiform (km)		Convective/Stratiform (km)	
GCE	75/55	89/49	13/70	19/64
C&H	72/56	87/50	12/72	17/67
Xu	79/51	93/45	14/69	20/64
CA (20 km)	76/52	91/47	21/59	28/54
Steiner	87/41	100/37	30/49	36/45
Vt-W	99/31	110/29	31/52	40/43
Average	81/47	95/43	20/62	27/56

Table 5 - PRESTORM/4th

	GCE	C&H	Xu	CA20	Steiner	Vt-W
Condensation	83.6	70.6	92.5	88.7	97.2	97.6
Evaporation	48.1	43.6	55.9	47.7	72.3	76.5
Deposition	46.6	34.7	53.1	44.4	62.3	70.4
Sublimation	22.4	21.5	25.7	25.2	33.8	41.3
Freezing	80.8	65.0	87.1	79.5	96.8	96.7
Melting	51.8	42.5	61.9	51.5	80.2	81.3

Table 6 PRESTORM/PDA

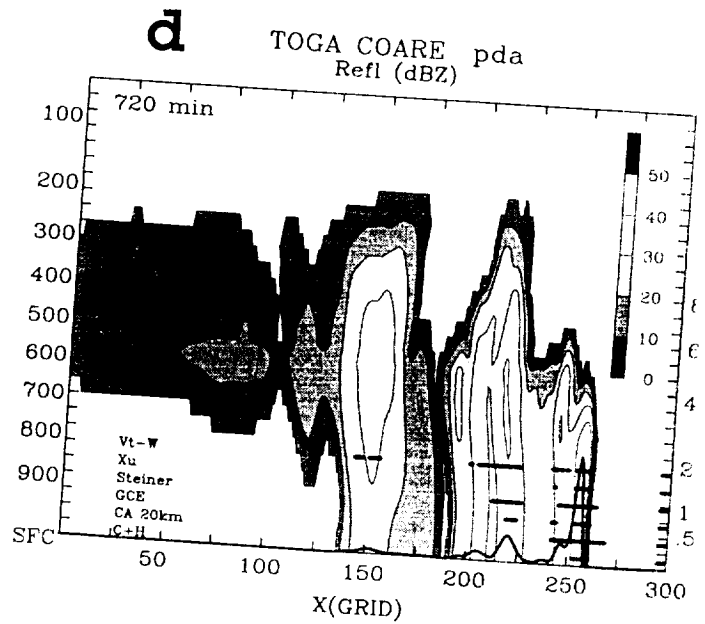
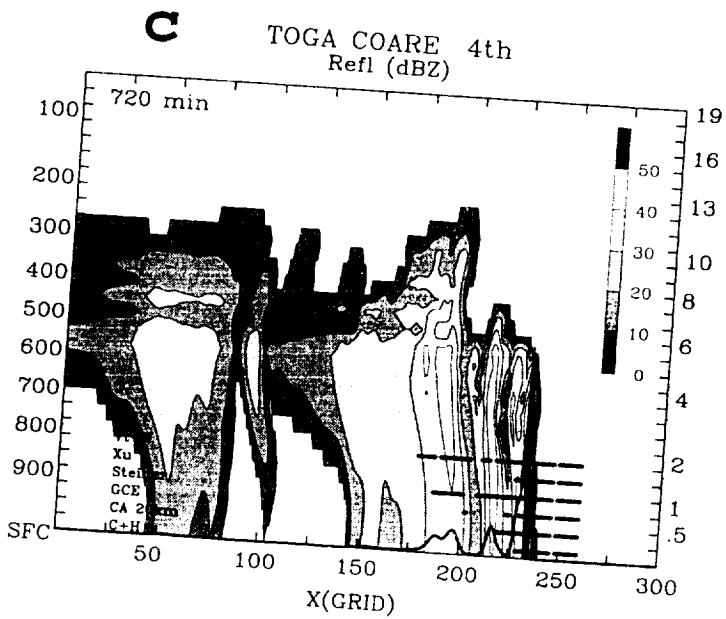
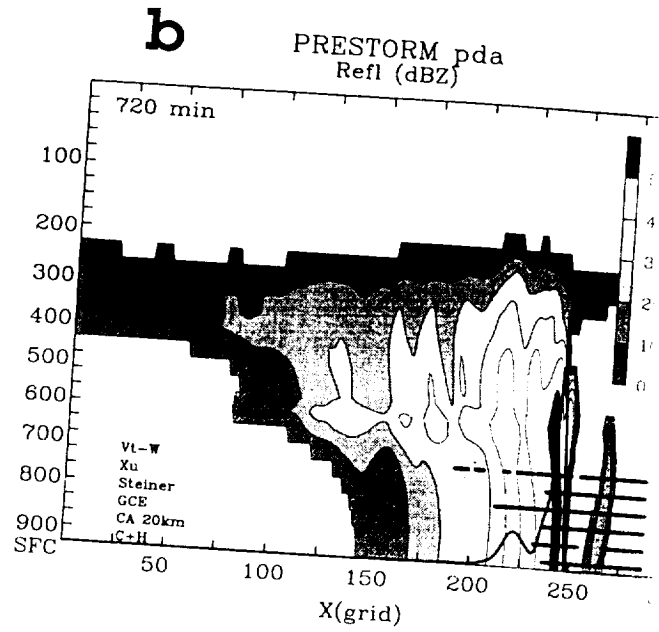
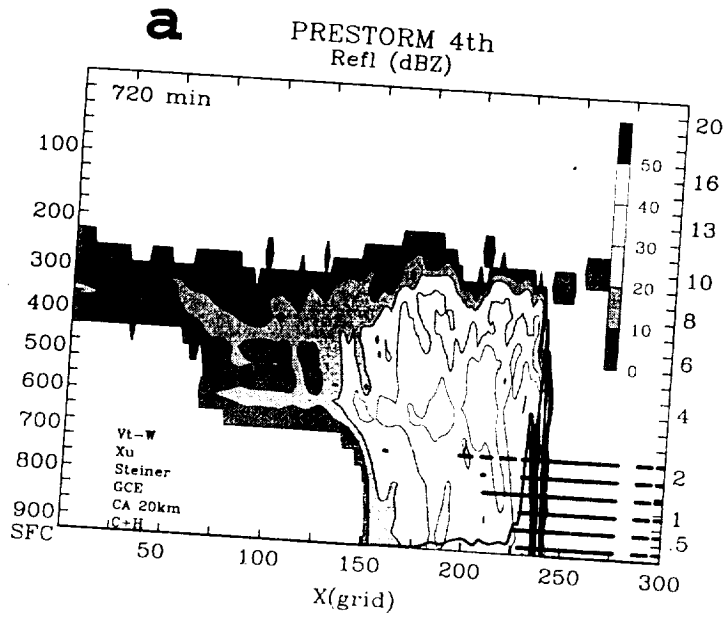
	GCE	C&H	Xu	CA20	Steiner	Vt-W
Condensation	84.5	72.6	94.1	90.8	97.5	97.8
Evaporation	55.2	51.6	64.9	56.8	79.1	80.6
Deposition	36.7	30.8	43.6	36.9	51.2	56.6
Sublimation	17.8	17.3	21.1	19.9	27.2	33.5
Freezing	85.4	77.1	91.3	86.0	97.7	97.7
Melting	61.3	56.0	71.7	61.4	86.8	85.6

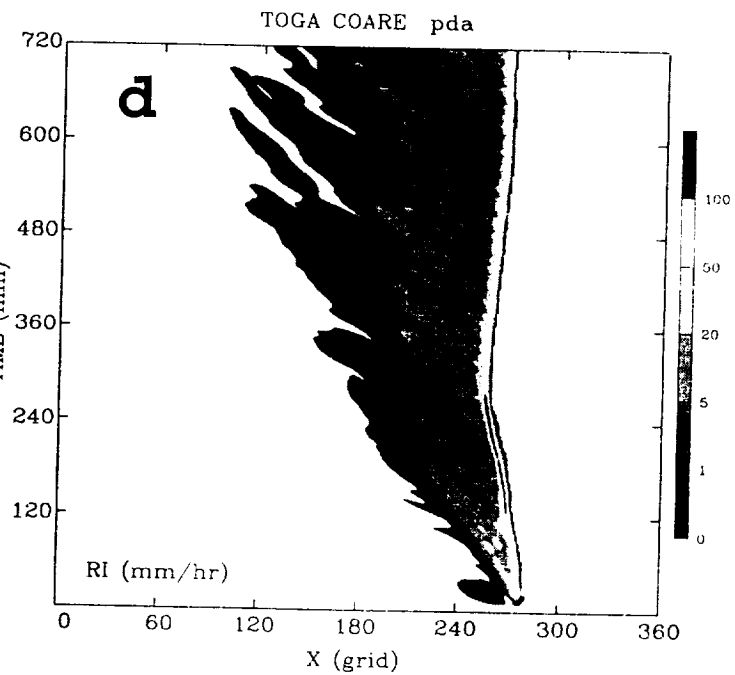
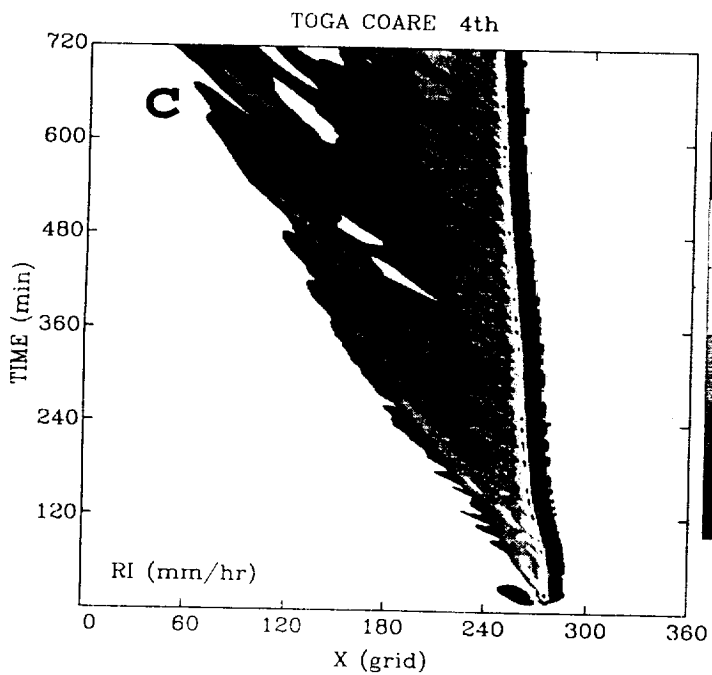
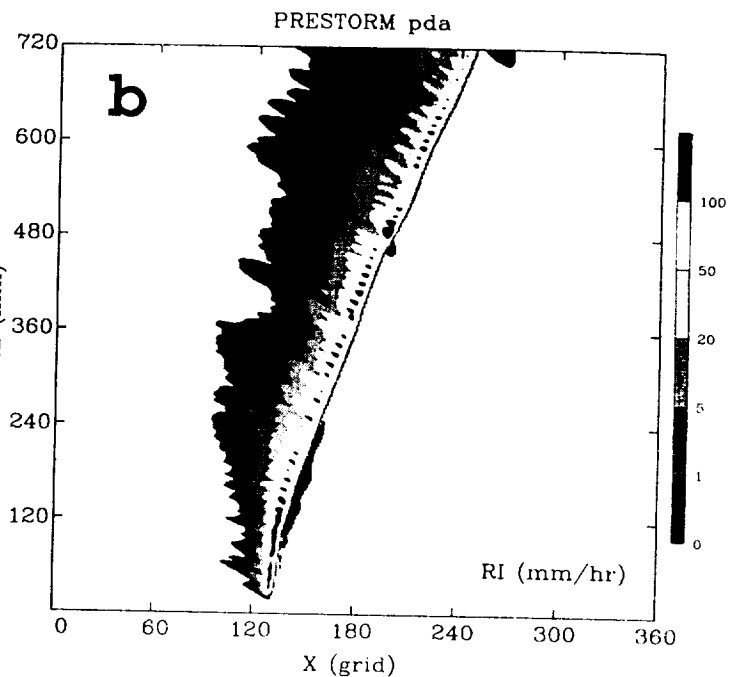
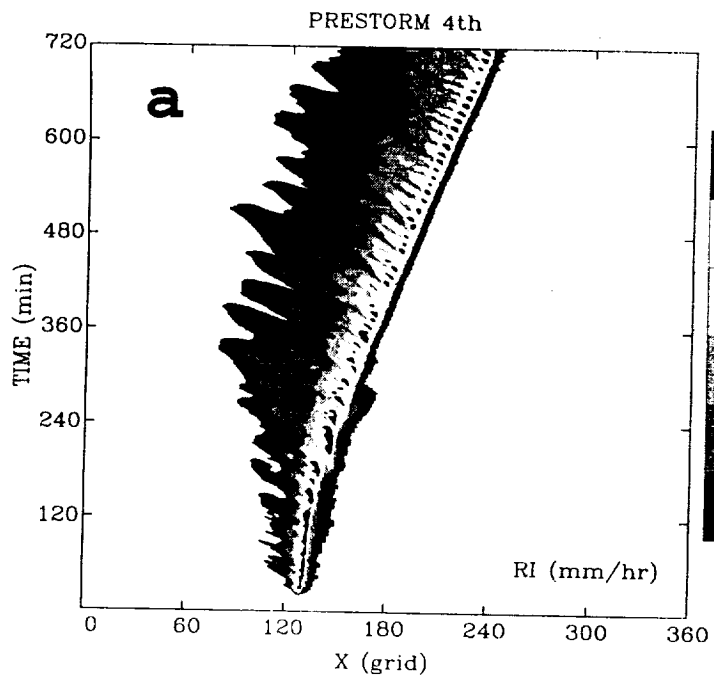
Table 7 - TOGA COARE/4th

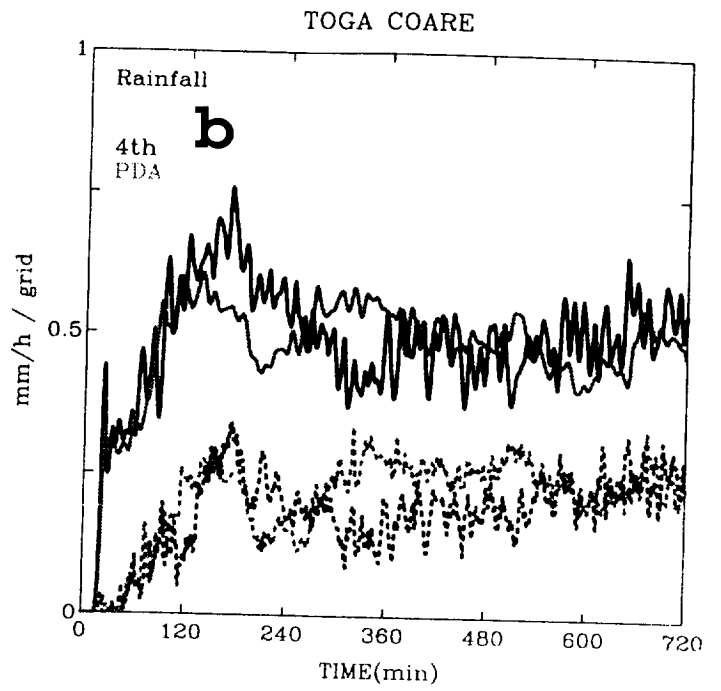
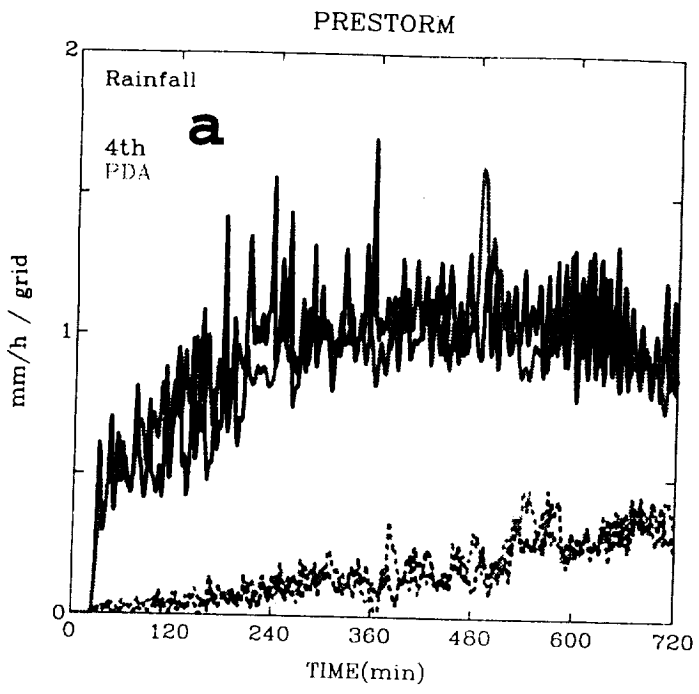
	GCE	C&H	Xu	CA20	Steiner	Vt-W
Condensation	70.4	60.2	74.1	79.4	89.9	92.0
Evaporation	26.4	22.8	29.4	41.4	58.6	54.7
Deposition	5.6	3.8	18.1	11.7	41.4	53.7
Sublimation	7.8	4.6	15.0	18.5	48.3	48.5
Freezing	24.0	12.6	40.5	46.5	79.6	85.9
Melting	3.9	3.4	13.7	12.3	45.5	48.2

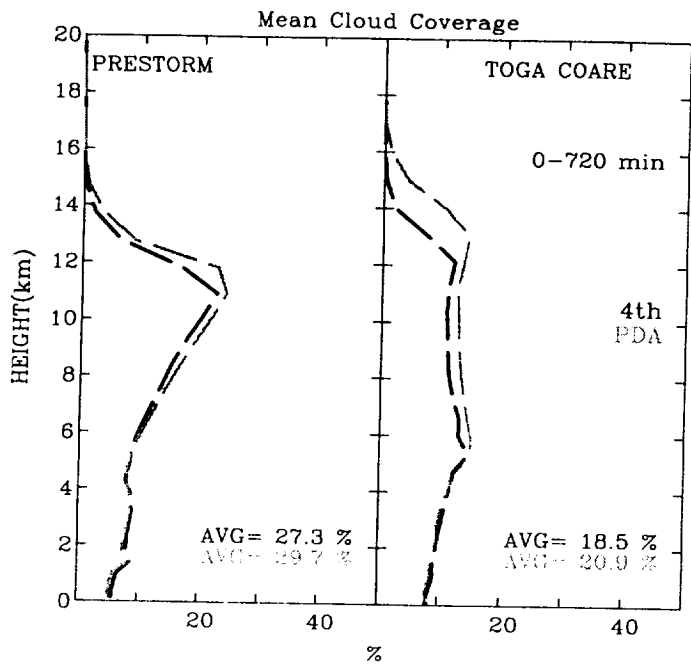
Table 8 TOGA COARE/PDA

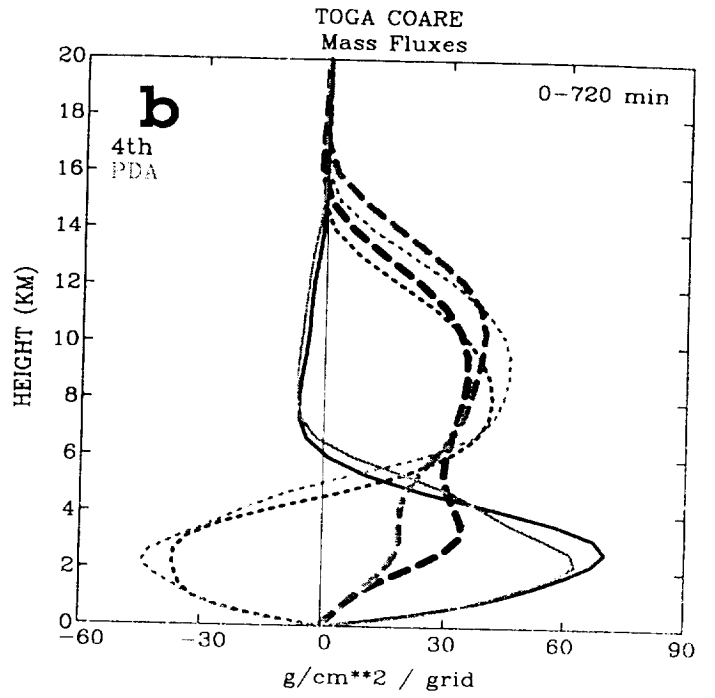
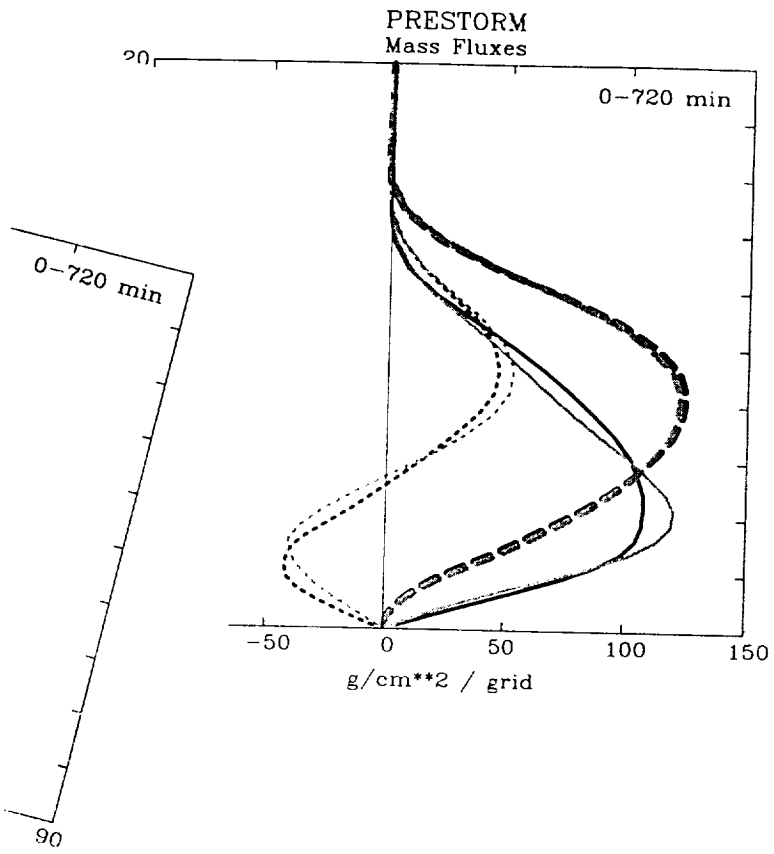
	GCE	C&H	Xu	CA20	Steiner	Vt-W
Condensation	67.3	54.7	70.3	71.0	82.1	90.1
Evaporation	23.4	20.1	27.7	39.7	56.7	57.9
Deposition	6.4	3.7	24.7	11.6	43.0	67.5
Sublimation	4.9	2.6	11.1	12.1	36.2	42.7
Freezing	39.4	24.0	54.6	46.6	74.3	92.1
Melting	7.3	4.8	18.6	18.7	49.8	61.2

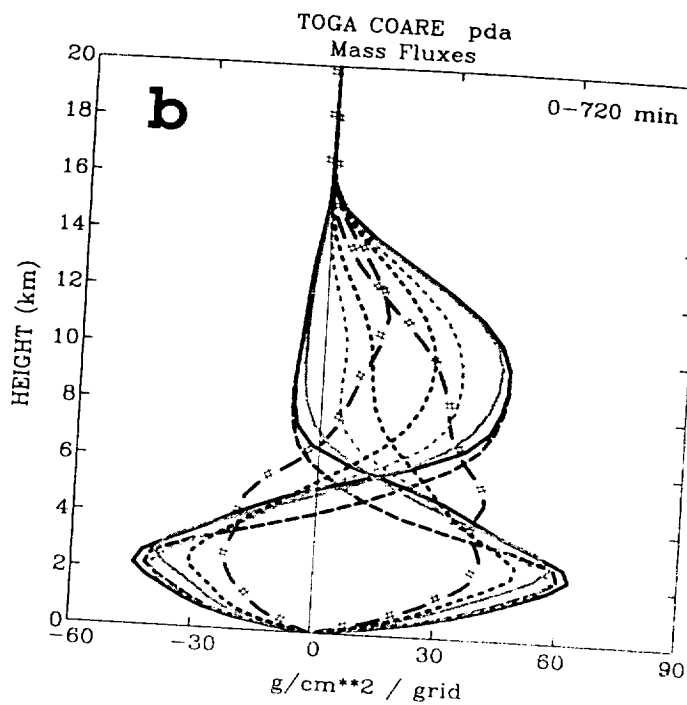
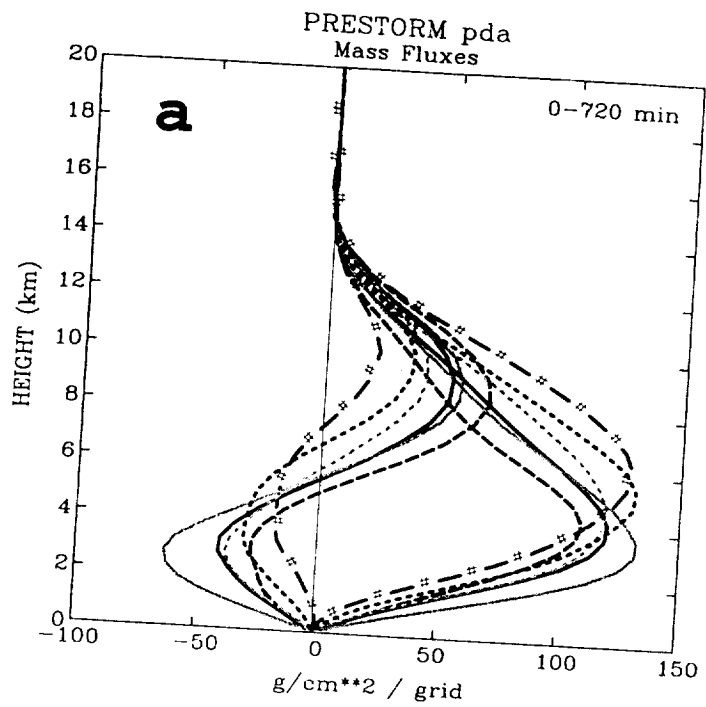












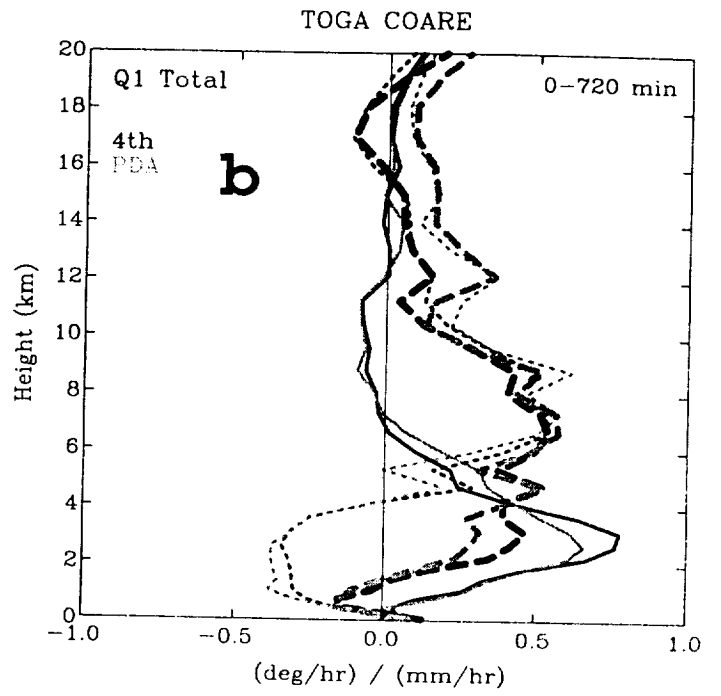
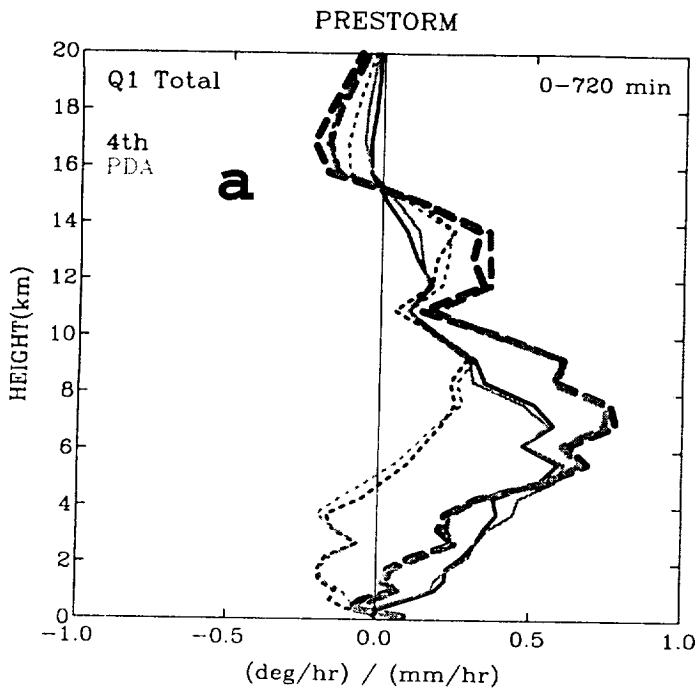
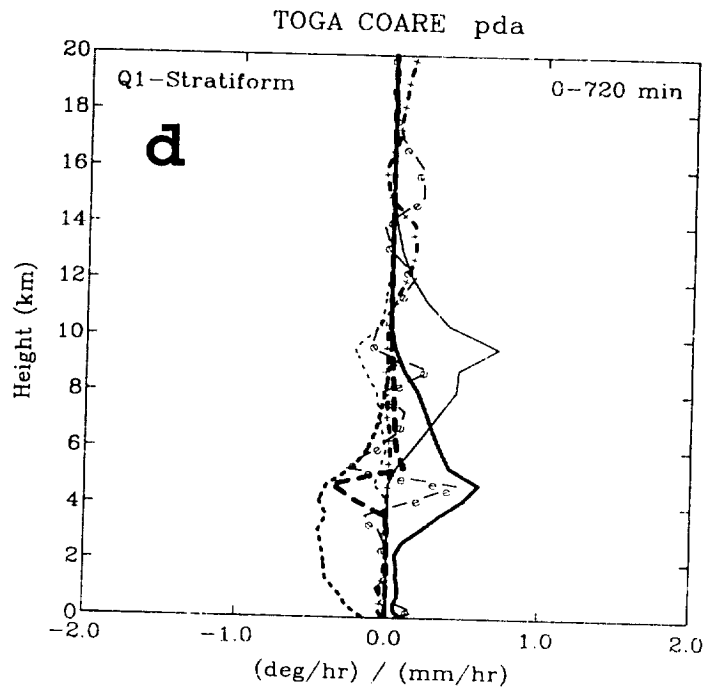
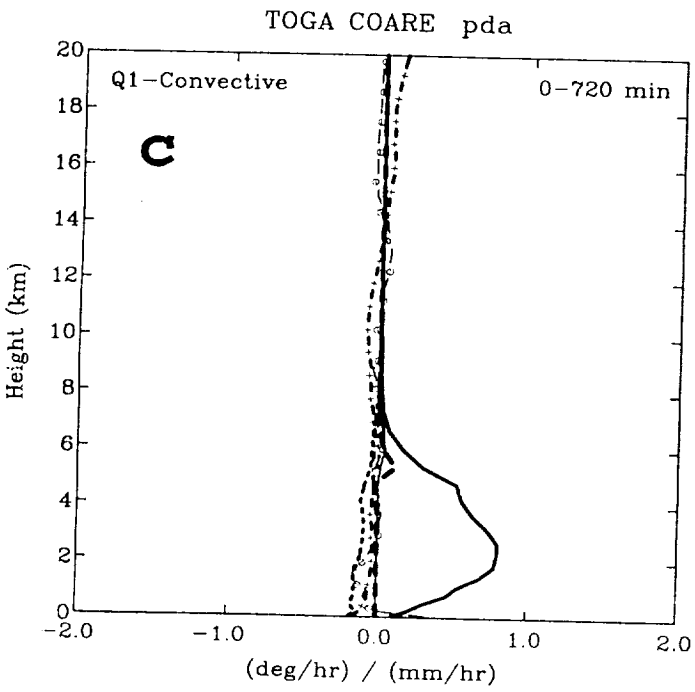
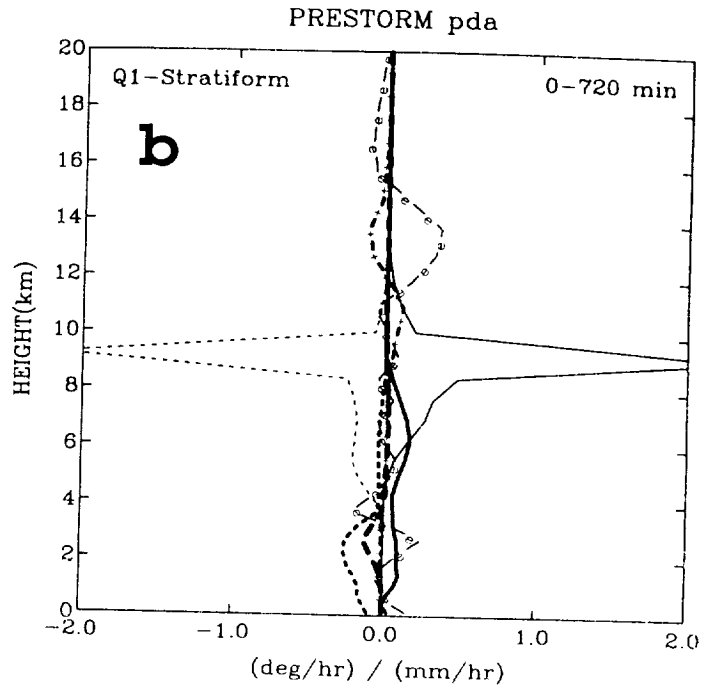
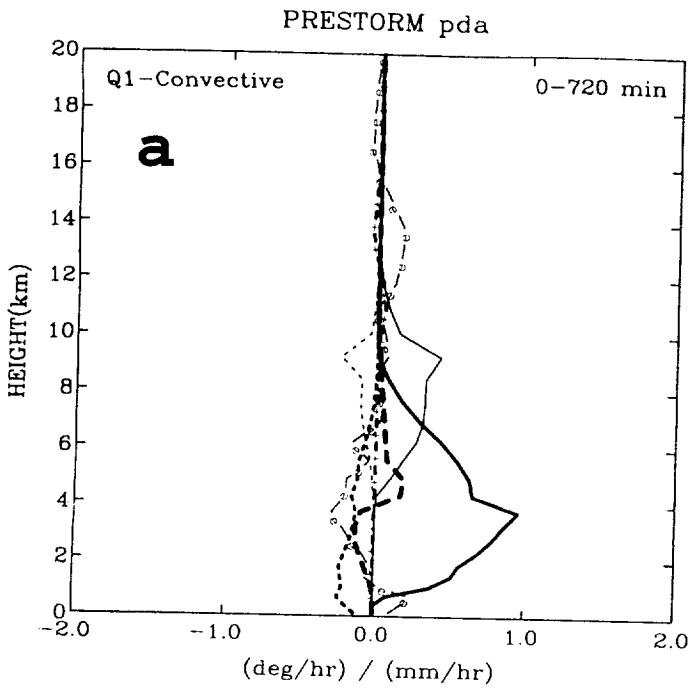
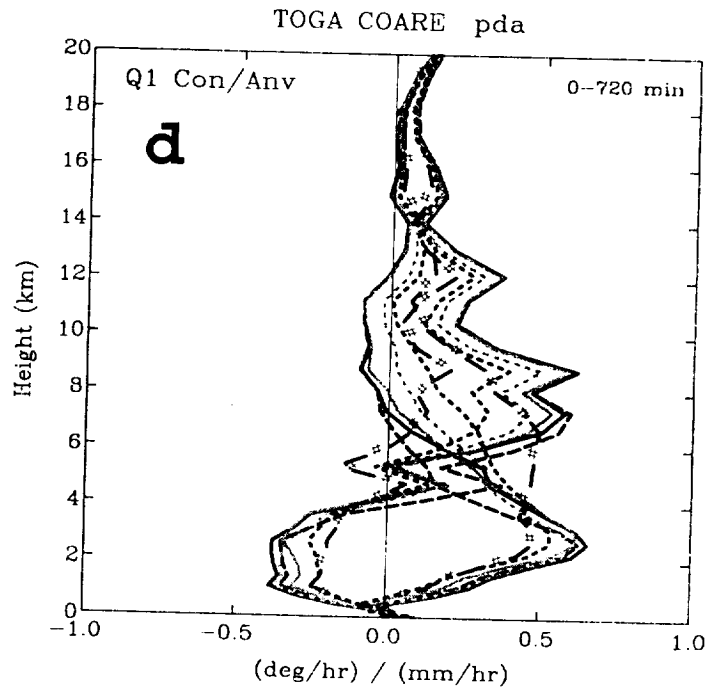
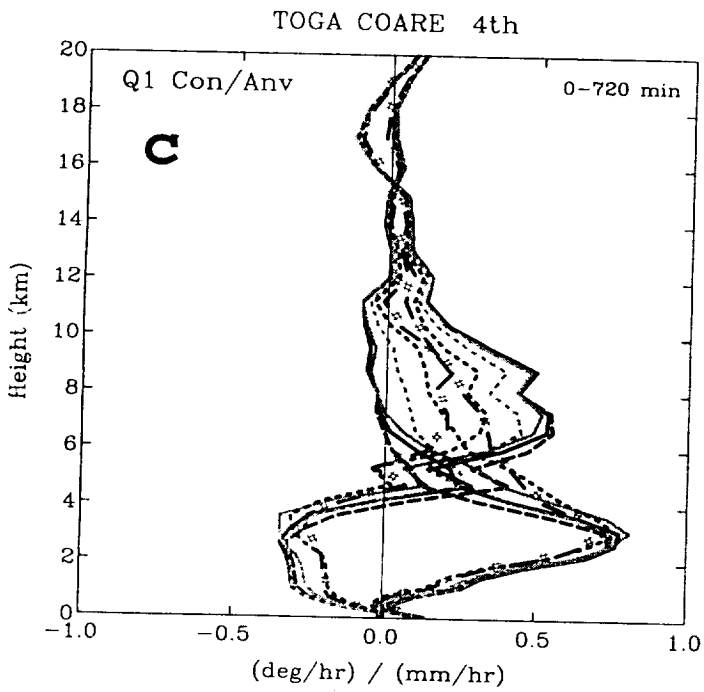
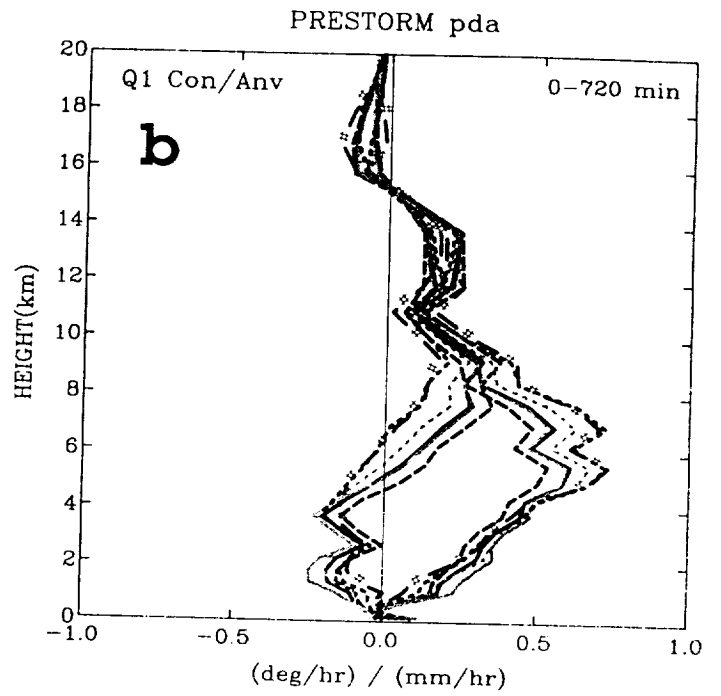
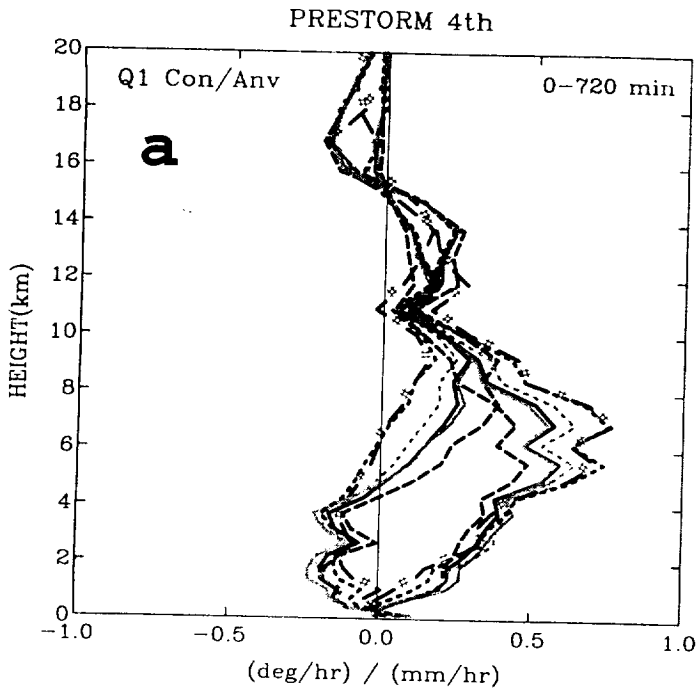
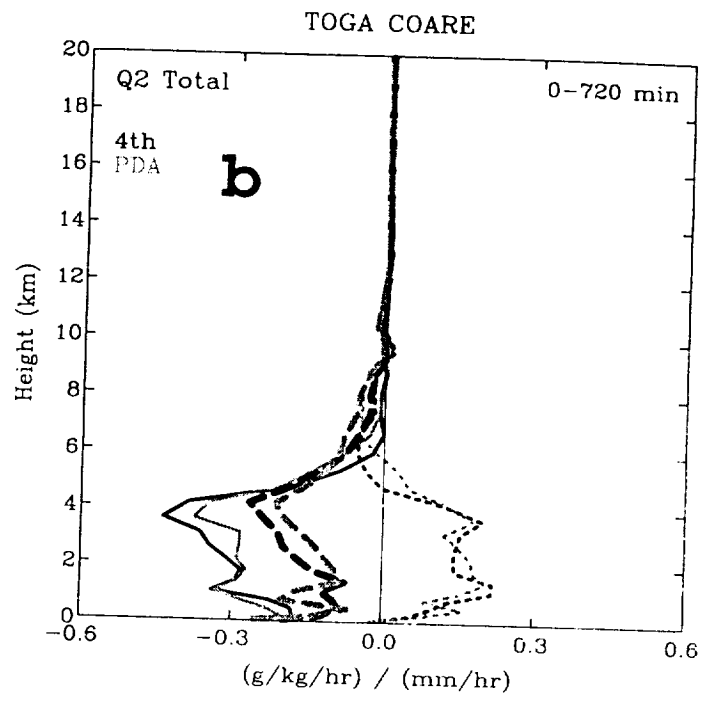
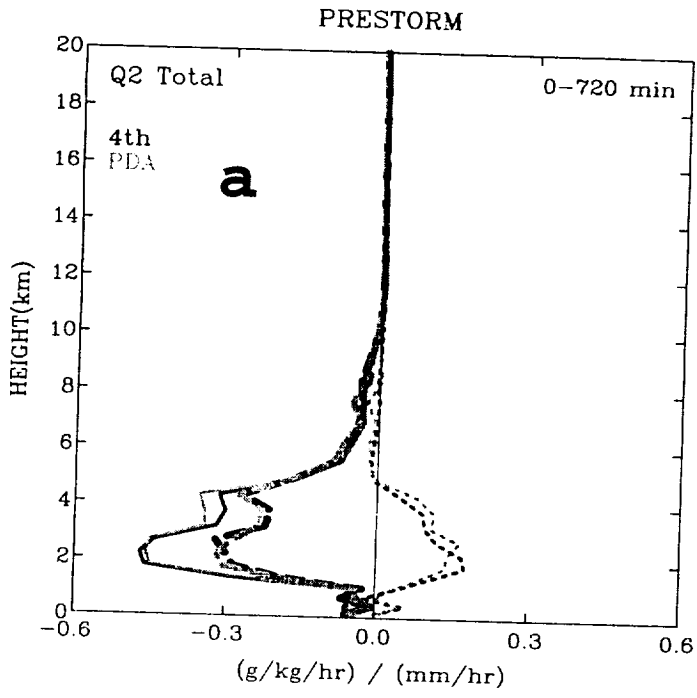


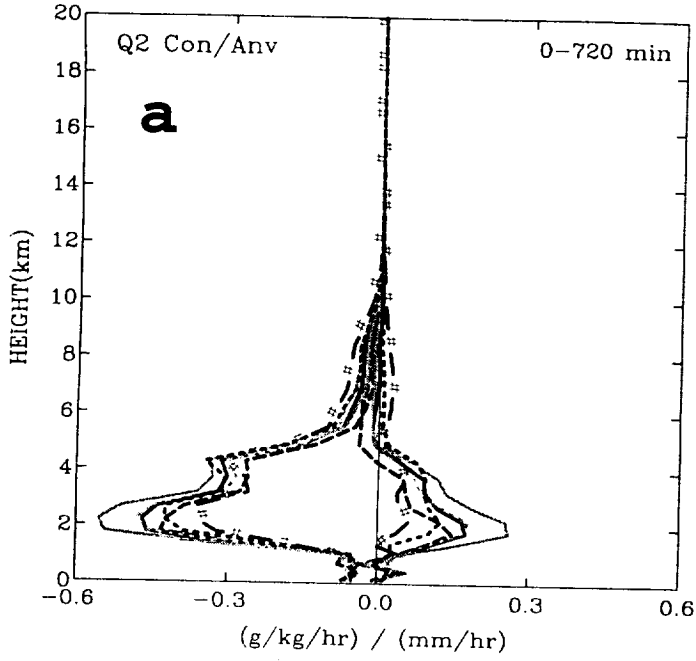
Fig. 1



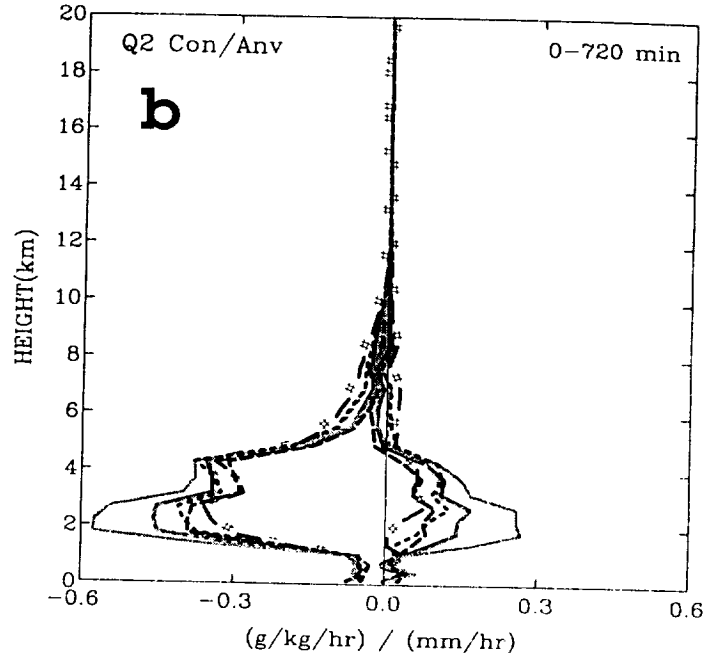




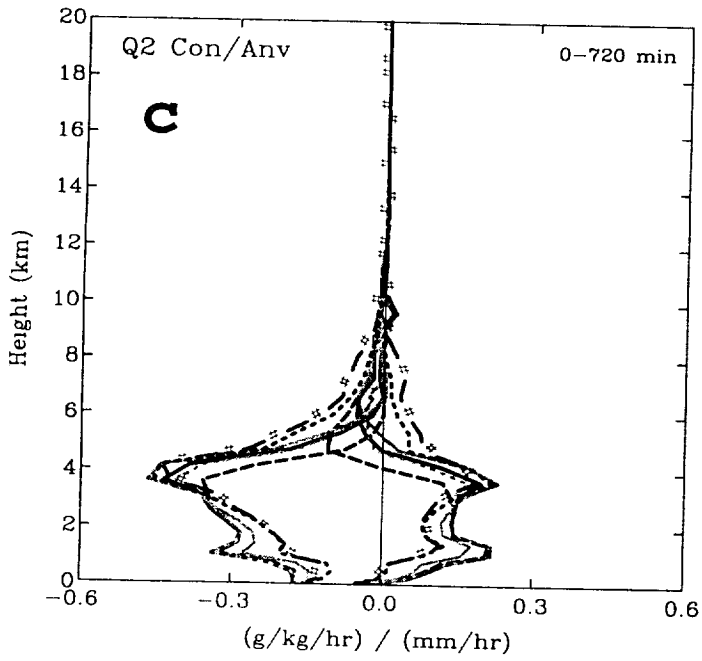
PRESTORM 4th



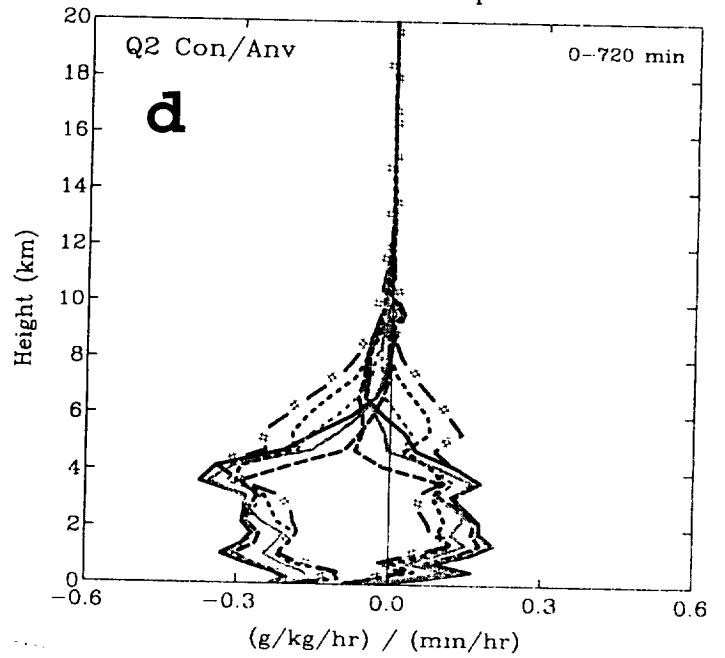
PRESTORM pda

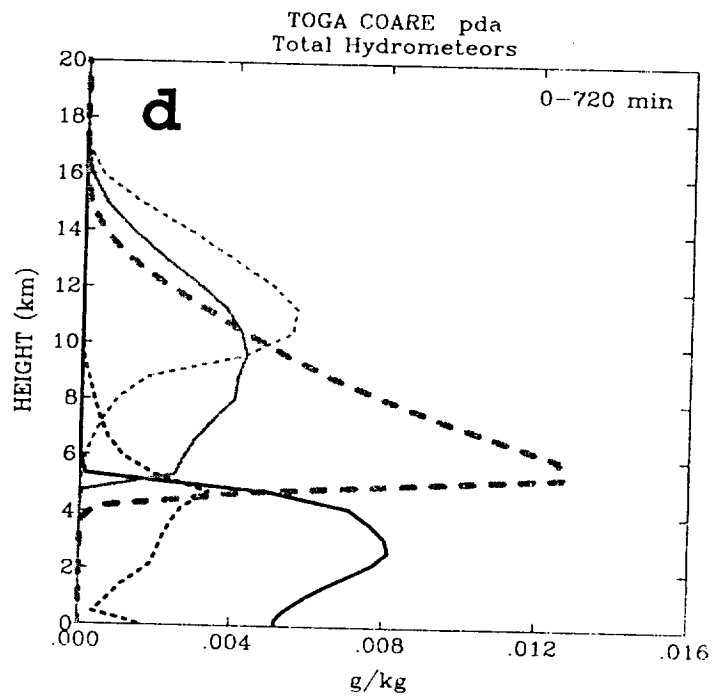
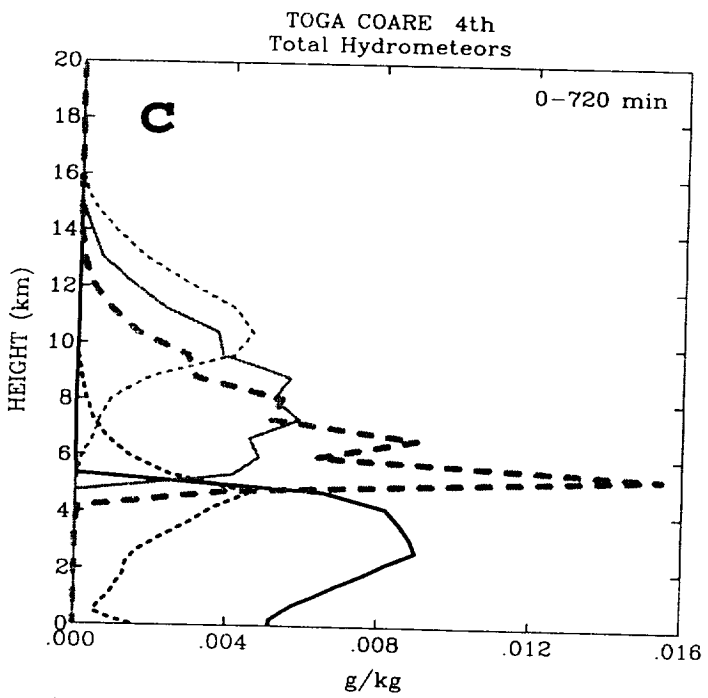
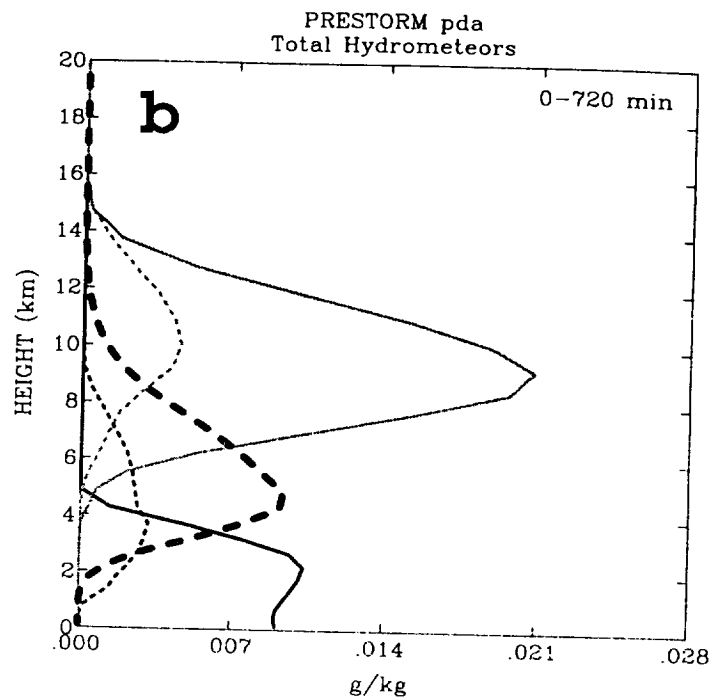
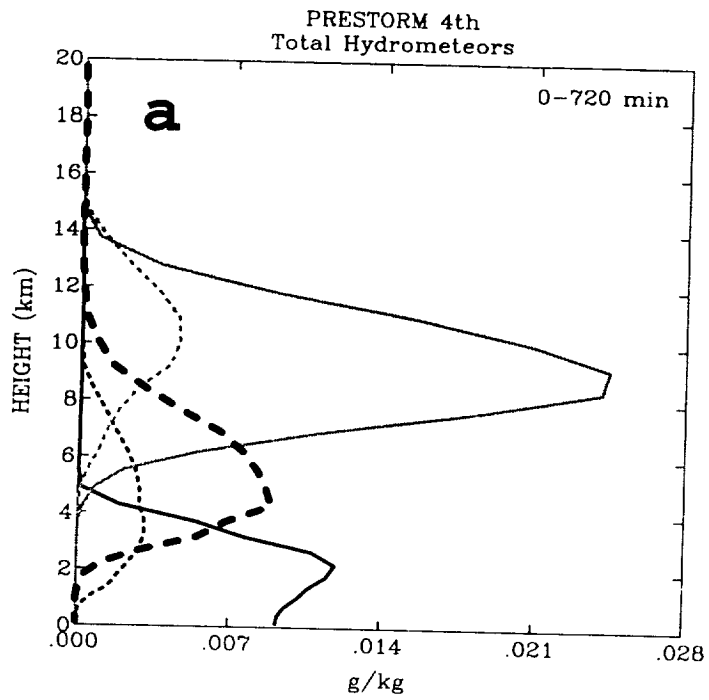


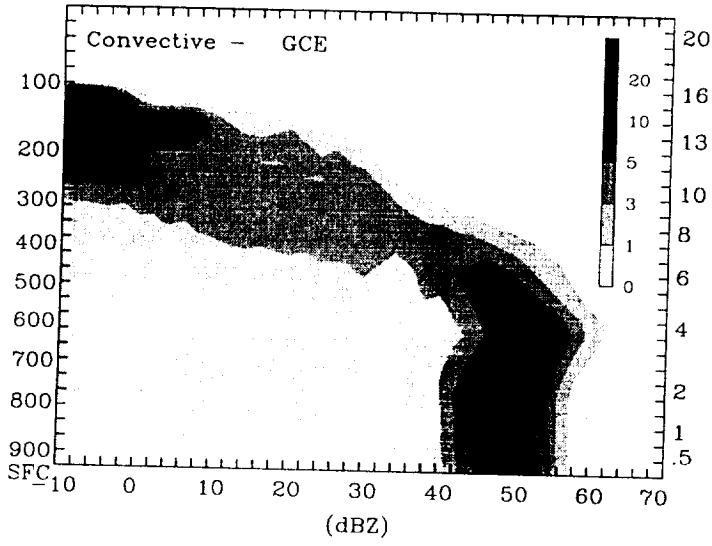
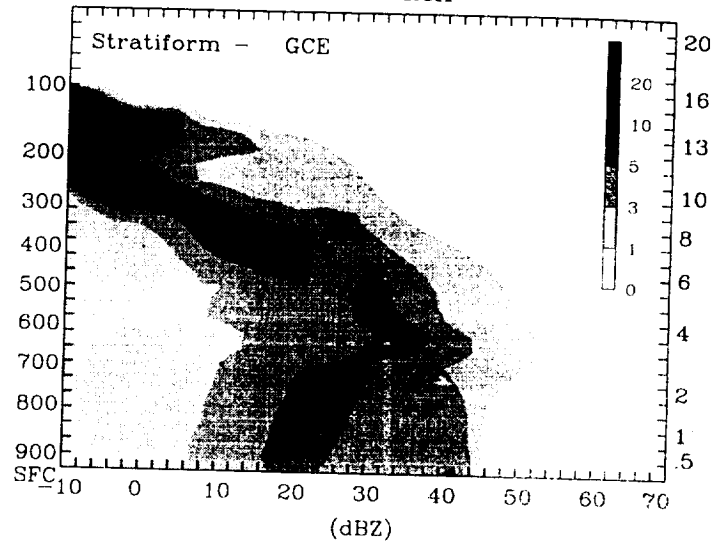
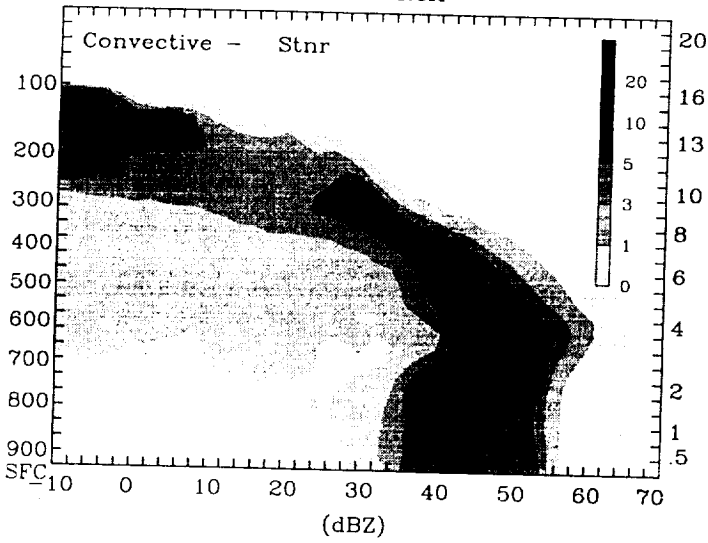
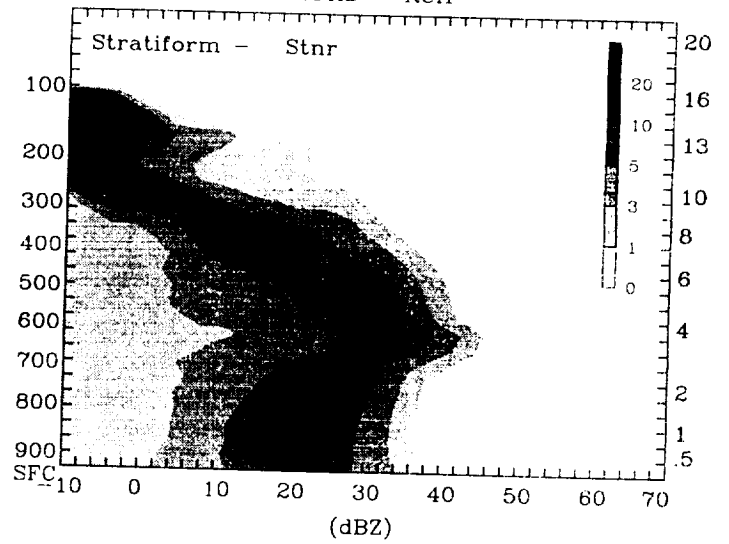
TOGA COARE 4th

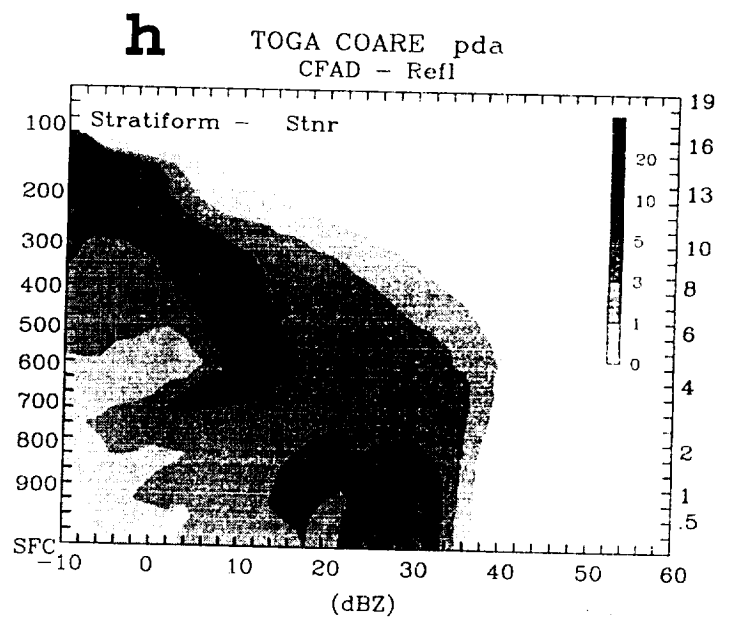
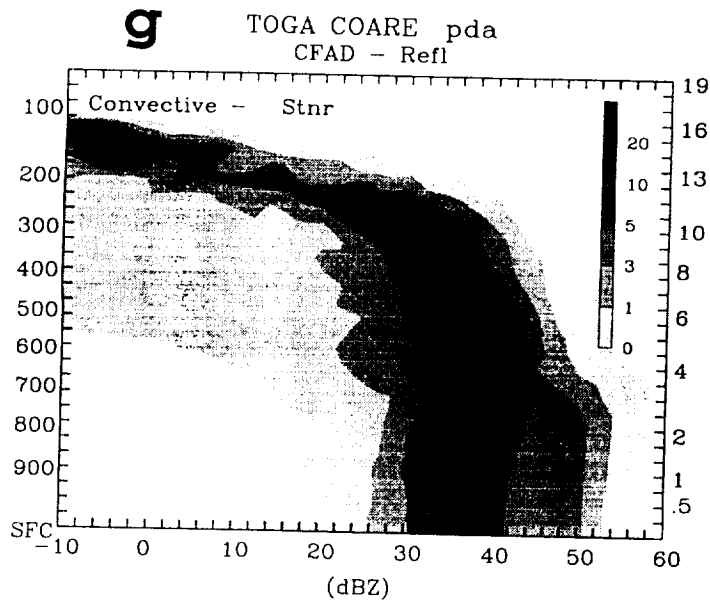
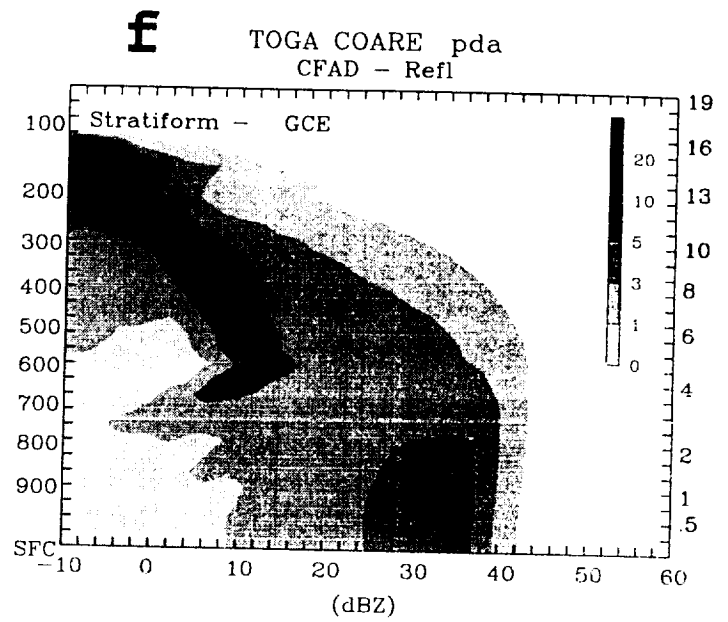
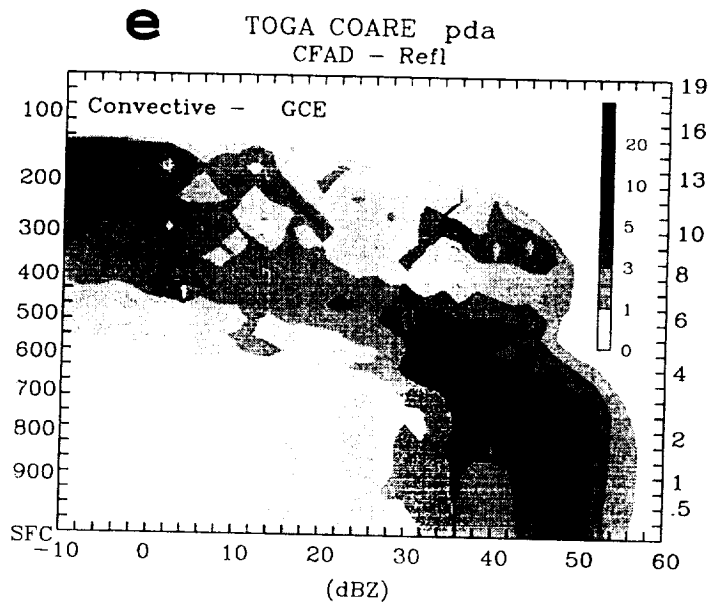


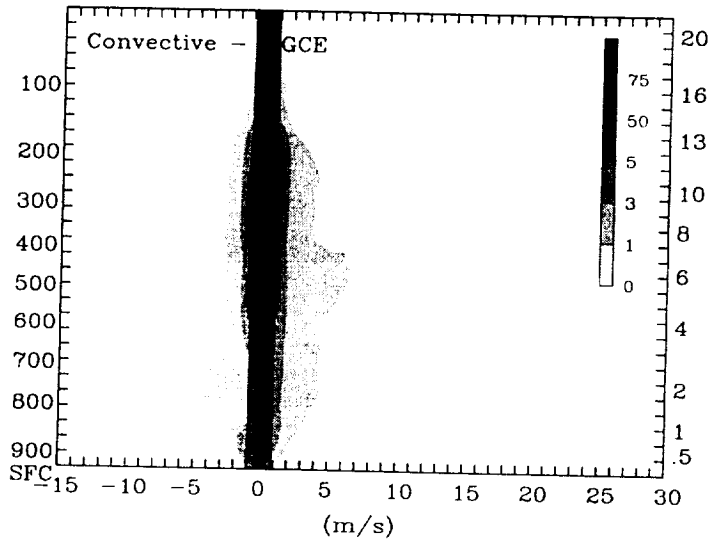
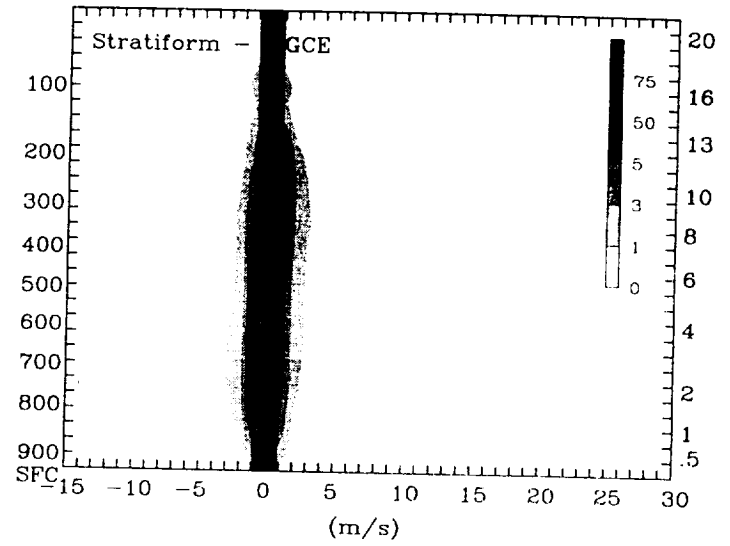
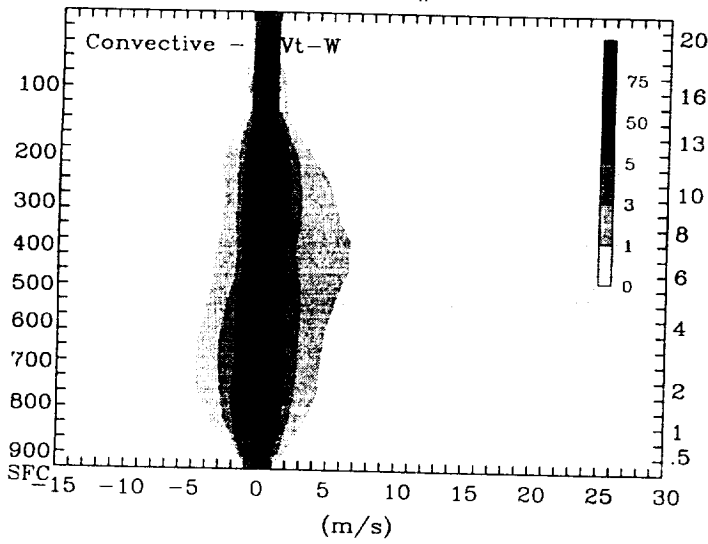
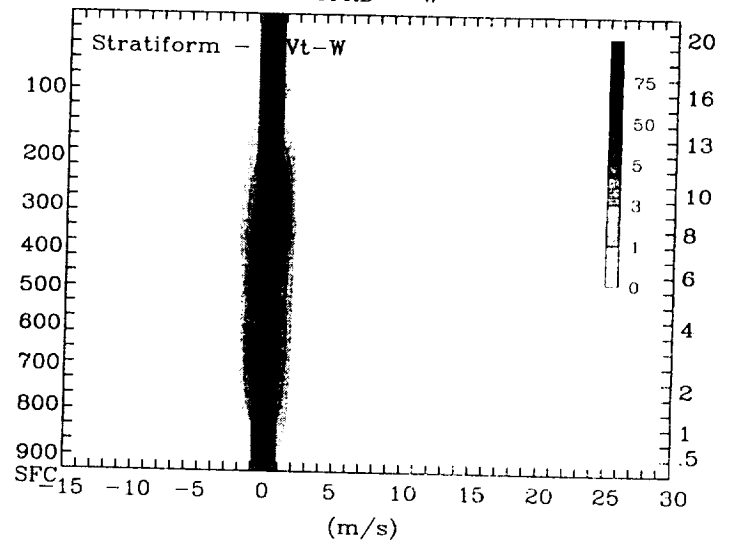
TOGA COARE pda

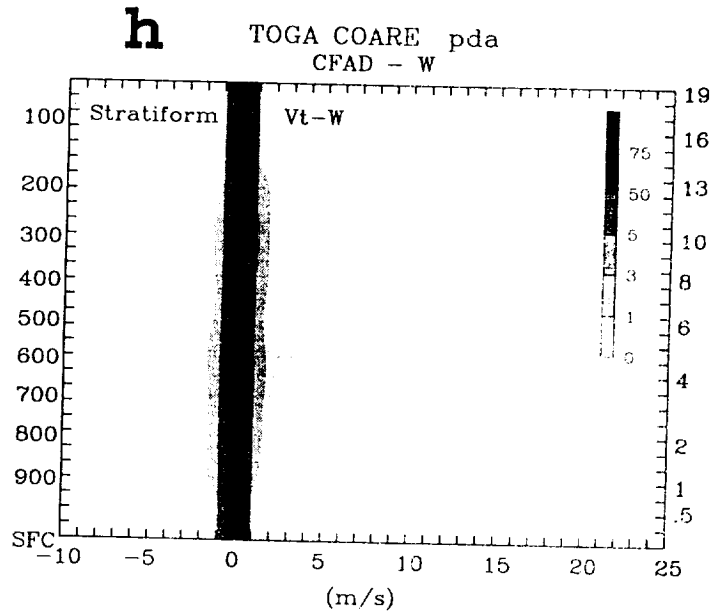
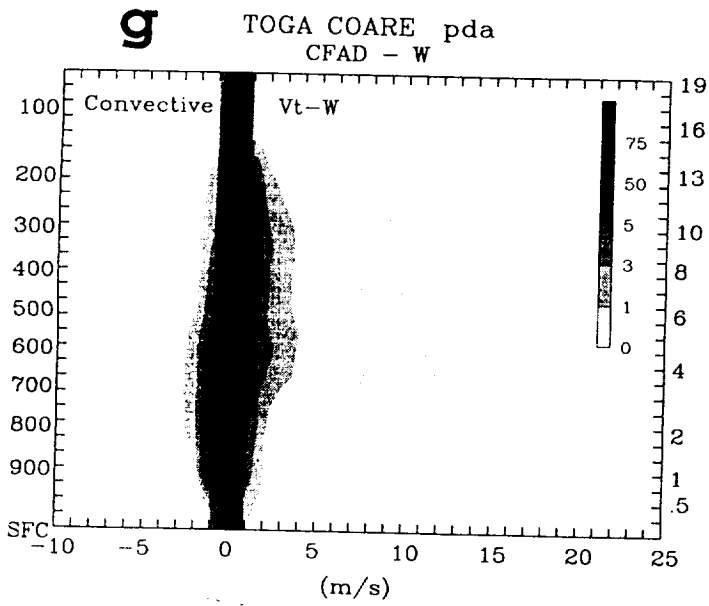
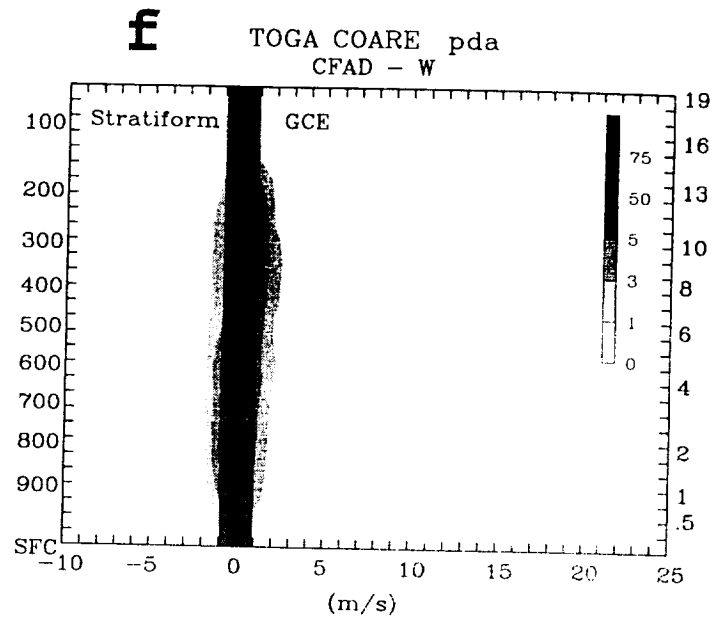
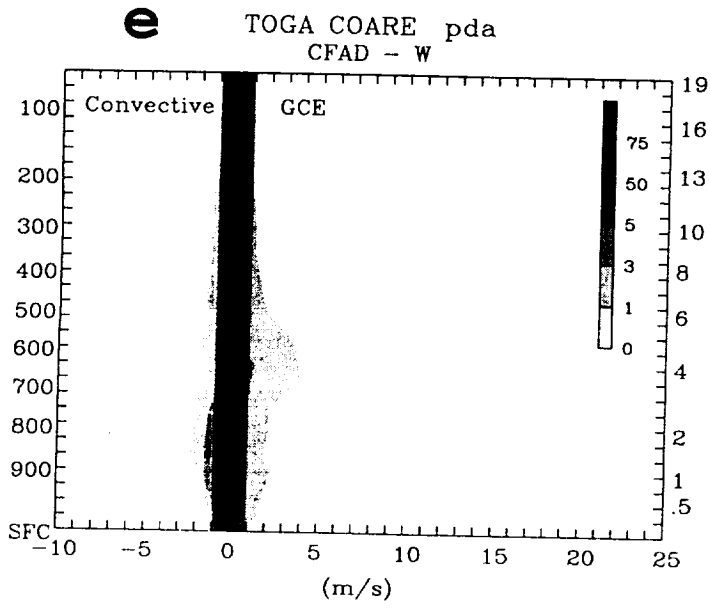


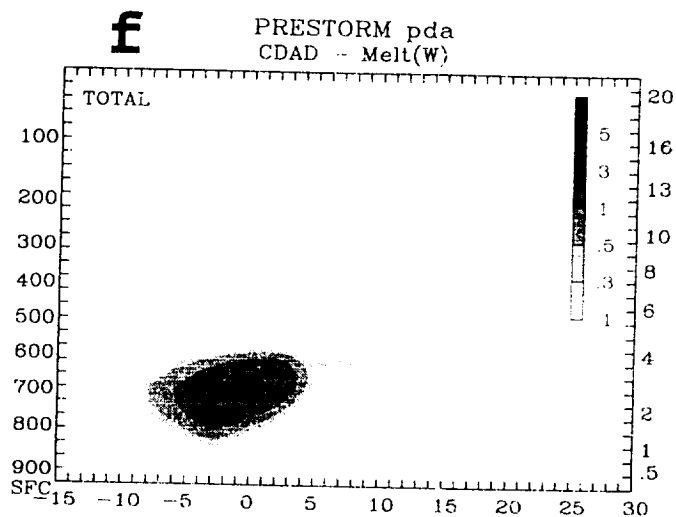
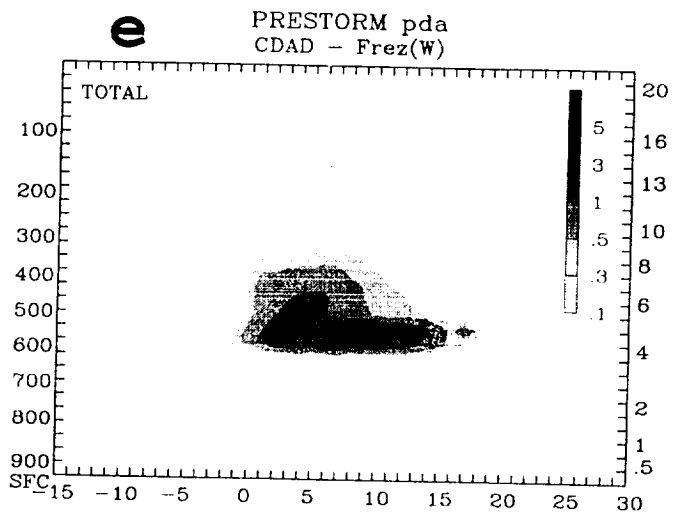
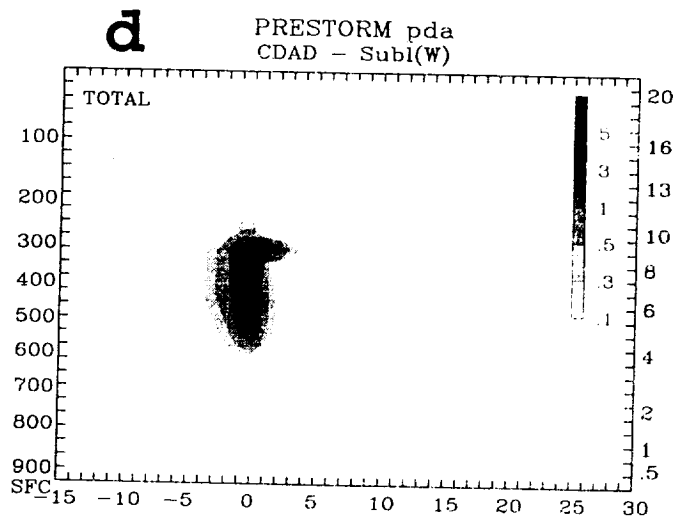
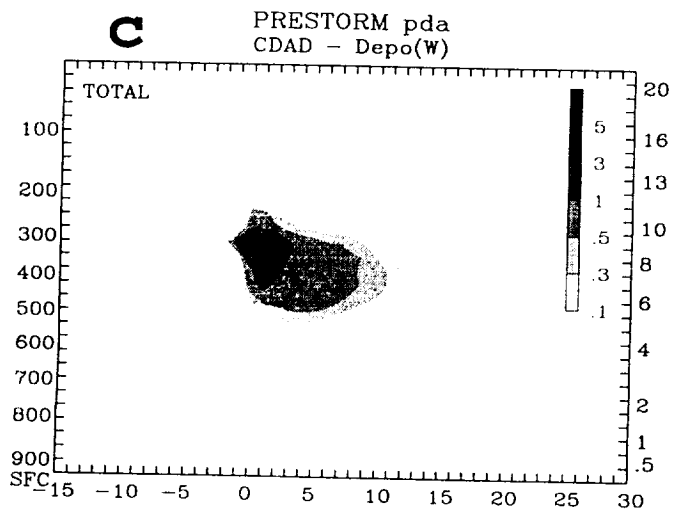
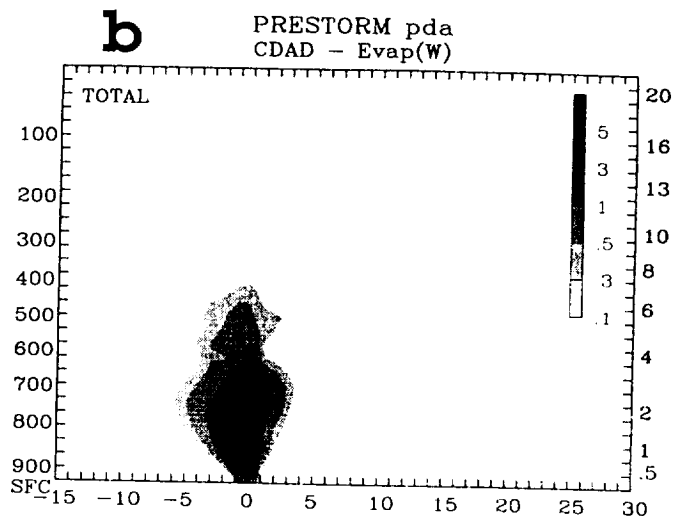
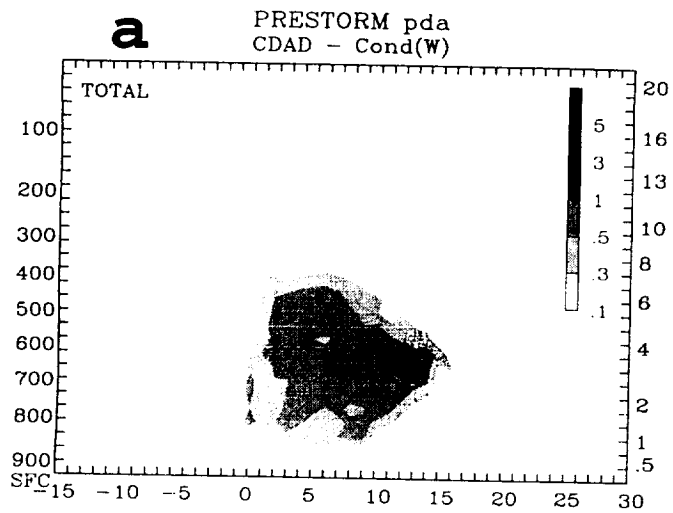


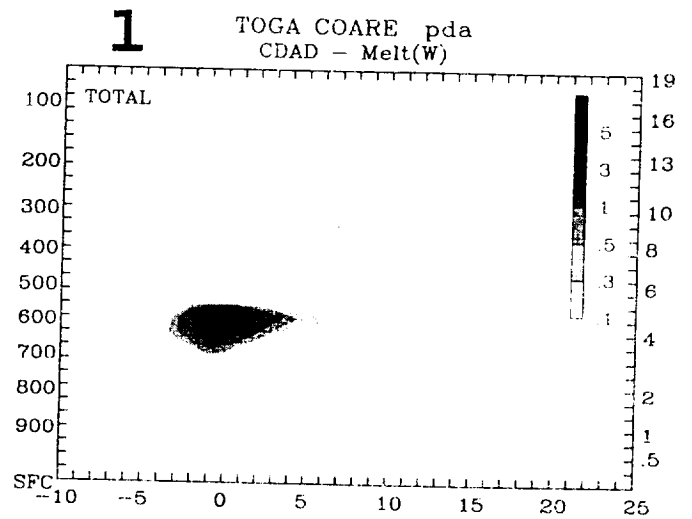
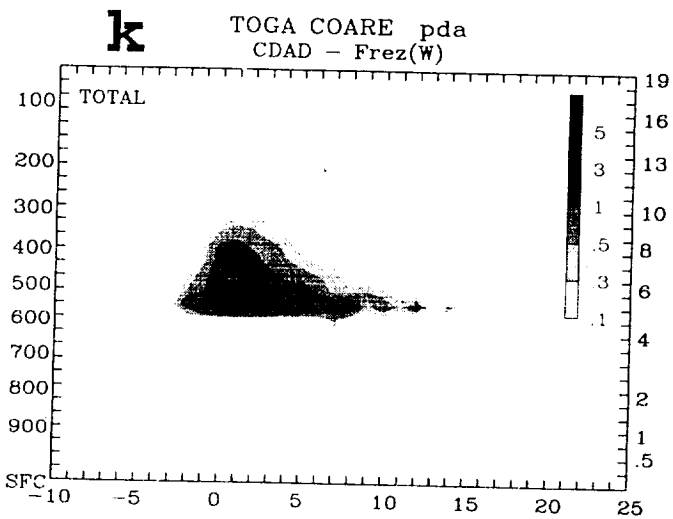
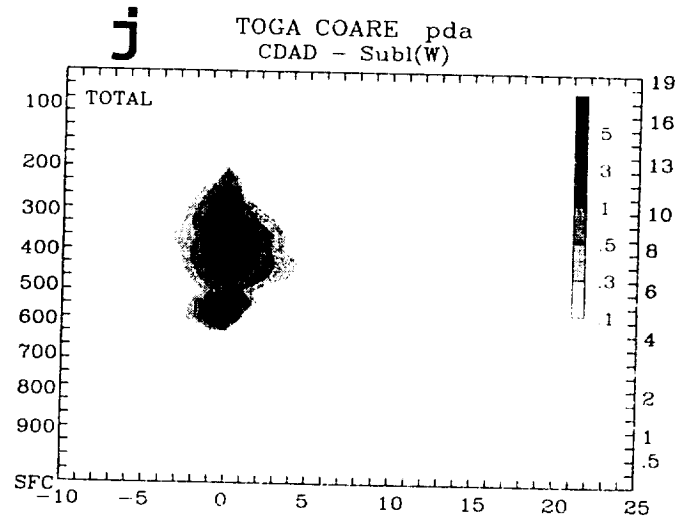
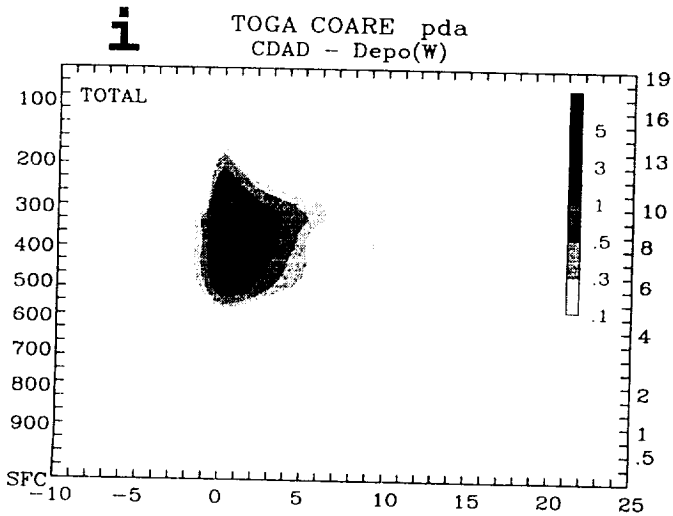
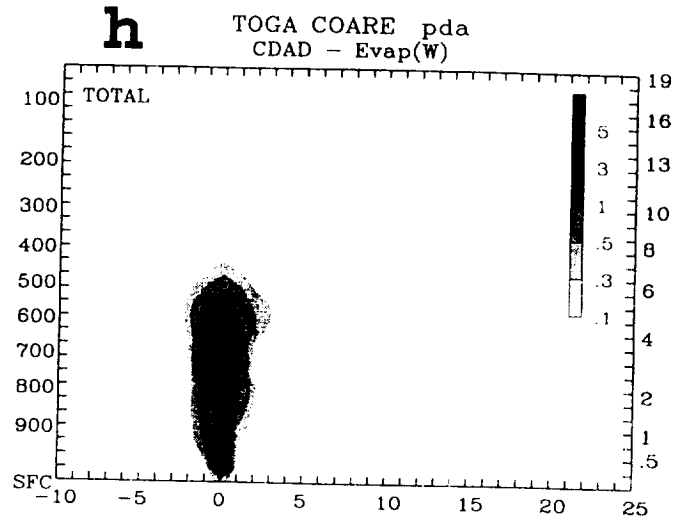
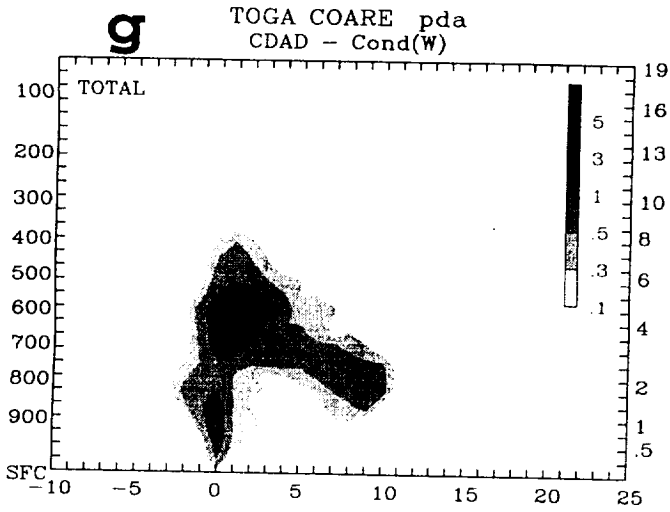
aPRESTORM pda
CFAD - Refl**b**PRESTORM pda
CFAD - Refl**c**PRESTORM pda
CFAD - Refl**d**PRESTORM pda
CFAD - Refl



aPRESTORM pda
CFAD - W**b**PRESTORM pda
CFAD - W**c**PRESTORM pda
CFAD - W**d**PRESTORM pda
CFAD - W







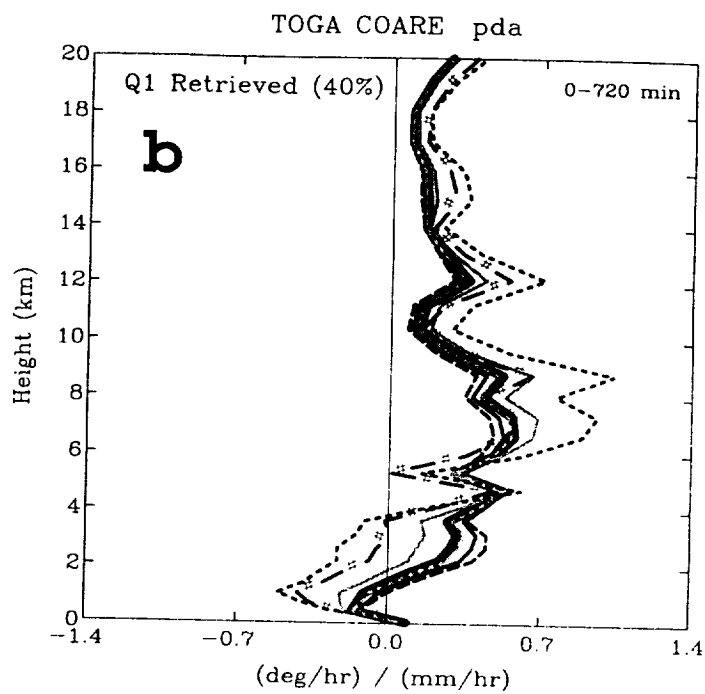
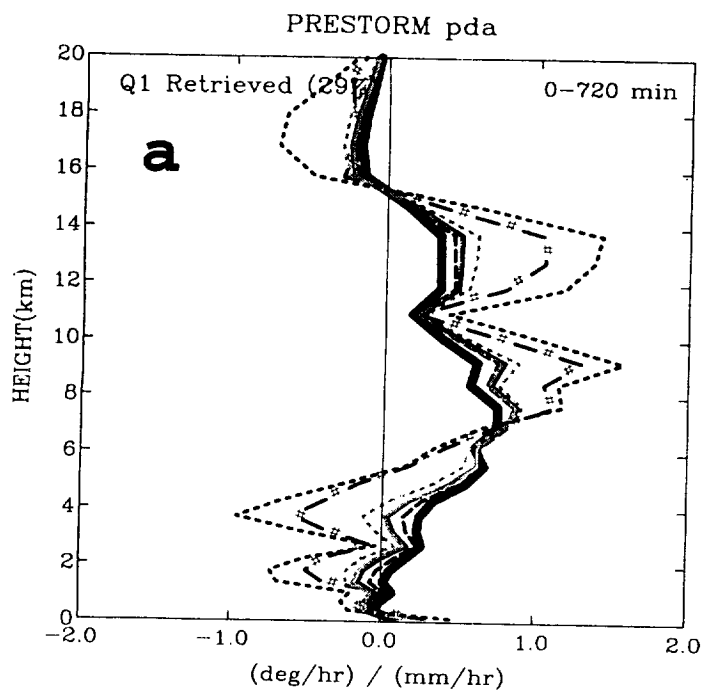


Fig. 16

